



Method Article

Quantum field lens coding and classification algorithm to predict measurement outcomes

Philip B. Alipour^{a,*}, T. Aaron Gulliver^a*Department of Electrical and Computer Engineering, University of Victoria, Victoria BC, V8W 2Y2, Canada*

ARTICLE INFO

Method name:

Quantum field lens coding and classification (QF-LCC)

Keywords:

Quantum double-field
QDF Transformation
QDF Lens coding
DF Computation
Entanglement entropy
N-qubit machines
Quantum fourier transform
Quantum artificial intelligence
Quantum lens distance-based classification

ABSTRACT

This study develops a method to implement a quantum field lens coding and classification algorithm for two quantum double-field (QDF) system models: 1- a QDF model, and 2- a QDF lens coding model by a DF computation (DFC). This method determines entanglement entropy (EE) by implementing QDF operators in a quantum circuit. The physical link between the two system models is a quantum field lens coding algorithm (QF-LCA), which is a QF lens distance-based, implemented on real *N*-qubit machines. This is with the possibility to train the algorithm for making strong predictions on phase transitions as the shared objective of both models. In both system models, QDF transformations are simulated by a DFC algorithm where QDF data are collected and analyzed to represent energy states and transitions, and determine entanglement based on EE. The method gives a list of steps to simulate and optimize any thermodynamic system on macro and micro-scale observations, as presented in this article:

- The implementation of QF-LCA on quantum computers with EE measurement under a QDF transformation.
- Validation of QF-LCA as implemented compared to quantum Fourier transform (QFT) and its inverse, QFT^{-1} .
- Quantum artificial intelligence (QAI) features by classifying QDF with strong measurement outcome predictions.

Specifications table

Subject area:	Computer Science
More specific subject area:	Decision sciences, statistical mechanics, energy, physics and astronomy: quantum computing, communications, particles and statistical physics
Name of your method:	Quantum field lens coding and classification (QF-LCC)
Name and reference of your original method:	P. B. Alipour, T. A. Gulliver (2023), A double-field computation model to simulate physical systems. doi: 10.2139/ssrn.4239321 distributed in Comp. SciRN Elsevier e-Journals e.g., <i>Comp. Theo.</i> 6 (2023) 10. The method from the associated article simulates quantum thermodynamic systems and implements QDF's theoretical aspects.
Resource availability:	Method's program code is supplied within this paper including links to validate results. Main dataset to download, as referenced is: https://doi.org/10.17632/gf2s8jkdfj .

* Corresponding author.

E-mail addresses: phibal12@uvic.ca, philbaback_orbsix@msn.com (P.B. Alipour).

Data description

In this research, the QF-LCA data are used from the related articles [4–6] representing simulated events as state and phase transitions (STs and PTs) in the QDF [4] and DF lens coding [6] system models, to evaluate and verify EE results from [6]. Tables 1 and 2 present the results summary where the measurement data, as in [5], are analyzed to validate the method proposed in this paper. The data are gathered from quantum measurement points in a proposed QDF system model which is implemented as a QF-LCA on an N -qubit machine.

Method details

System models

The system models from [4,6] involve three distinct components: the four measurement variables (fmv), a QDF, and a transition probability measure. The fmv are: i. an interaction length-based scalar κ that provides information on the system state, ii. a pairwise interaction distance relative to, iii. a position taking the quantum state of a pairwise particle interaction, and iv. the correlation length between the states of a particle pair. The fmv are measured from a QDF system which is simulated by a DF computation (DFC) algorithm [5,6].

A system model was proposed from a theoretical perspective as a quantum game to present QDF transformations [4]. Then the experimental model was proposed to implement the theory as a QDF lens heat engine, which is simulated by a DFC algorithm [6]. From there, the QF-LCA was formulated to observe, predict events in the system and control it to evaluate the algorithm through calculating EE, given a QDF transformation. The three distinct components for the empirical model lead to EE measure as a result of analyzing the data [5] on the ST probability measurement. From [6], the QDF lens coding products, such as QL focused and defocused probability distributions were introduced as convex lens, concave lens and a combination of convex and concave lens products, Table 1. These products were evaluated by calculating EE. Finally, QDF was implemented through a qubit coding method on N -qubit machines, which is the focus of this article. This article provides a summary of the previous steps to the point of implementation of an equivalent quantum circuit representing QF-LCA, as well as training the algorithm based on a quantum lens distance-based classification.

The supporting information is available from [6], where EE is determined between two (sub)systems A and B . This measure reveals where entanglement is expected between A and B as pairwise states on a scale of length $L \rightarrow L_{\mathcal{E}}$, where $L_{\mathcal{E}}$ is the entanglement length discussed in the method's EE measurement choice on p. 9.

A thermodynamic system simulated by DFC [6] is shown in the lower Fig. 1, which is based on the theoretical, upper Fig. 1. Measurements are done within the internal system B after sampling particles from external system A as the slit is closed. The slit opens after a lensing event on the sampled particles flowing out from B to A . In Fig. 1(c), photons are generated in a (10,3) single-walled carbon nanotube (SWCNT) as photonic probes (photoprobes) to conduct measurements. The CNTs are quantum light sources and detectors [14,23], which can generate probe fields and detect their photons from the system environment. A photoprobe's field can carry the average momentum of a BEC (Bose-Einstein Condensate), a non-BEC, or entangled BEC EPR (Einstein-Podolsky-Rosen) pairs as quantum information exchanged in the system [2,60–63]. This occurs in a laser cooling trap that maintains the frequent production of photons between an exciton energy level and ground state using SWCNTs while in contact with glass and a metal conductor, e.g., gold nano-particles in a lattice [7,23]. In Figs. 1(a, d), an external-internal entanglement of a paired particle is detected by observing the QDF transformation between A and B via a photodetector installed on a superconductor [6,31,32]. Fig. 1(e) shows there is a zero reactance to voltage drops between the two superconducting points in B , as temperature reaches a critical point (a PT). The resultant heat is absorbed by resistors in the CNT layer. As the frequency increases, the reactance of the capacitor decreases, and at a BEC point increases to let a proper readout of energy states of BEC atoms.

Fig. 1(f) shows a set of superposing particles entangle within the system, where photons in the probe's field are detected by photodetectors. Each measurement readout is from an entangled pair, where their entanglement is scaled between two or more QDF points [4, Eq. (6)]. The lenses in Fig. 1(g) function as a CNOT gate to (dis)entangle particles relative to Figs. 1(d)–(f) events contributing to a QPT. An adder Hamiltonian is formed by trapping particles that record which CNOT operator acted on the input state. The black dot is one of the CNOT operators that has acted on a possible 3-qubit input (CCNOT), while the rest remain in state $|0\rangle$ or BEC. The count is to measure how many times entanglement has occurred. The input denoting entanglement is the black dot, and the rest of the gates are the inverse (no entanglement or white dots). The photoprobes are later used to decompress the count by reading the state of the trapped particles e.g., EPR pairs into classical states.

In upper Fig. 1, the creation of a QDF is labelled in the heat engine's center based on the QDF lenses and their projection of states (lens products) from Fig. 1(g). The quantum information transfer for each projection is denoted by a qubit teleportation between an input state and an output state, and its inverse form to achieve this information is through superdense coding. The simulation and implementation of QDF is the core component of a QDF circuit and compatible with QFT transformations, as validated in Part II of Meth. Valid. p. 27. The validation of the QDF transformation theory is by observing the correlation within the variables of the DF measurement component $\langle kr \rangle$, [6]. This component for pairwise particles is measured between three or more particles as listed in Tables 2 and 4, followed by examples on distinguishable and indistinguishable states in Table 5. In this article, wherever the term "QDF circuit" is used, refers to quantum operations of the DFC model [6].

Entanglement entropy is used to determine a mixed state between at least a pair of particles as an entangled pair to yield information with certainty. We further compute locally distinguishable states using a third particle [4,31,63] from a lens product [6]. The

product represents the mixed state where the third particle exchanges energy with one of the paired particles (qubit communication). This results in a pure and separable state (a qubit readout) relative to a PT predicted with high probability in our method.

Method aim and objectives

The set of steps to simulate and implement the models must satisfy the following aim and objectives:

- **Aim:** Measure any thermodynamic system parameter based on entanglement coding and entropy.
- ⊗ The requirement is to simulate the scale of the observation of a given energy input $E_{\text{in}}|\Psi\rangle$ to the energy output $E_{\text{out}}|\Psi\rangle$ within the system, where Ψ is the wavefunction for a position-based particle, like a fermion inside a lattice Ising model [16,18], [12, Chaps. 3, 7].
- ⊗ If one or more particles are not participating in a refrigeration or combustion event (a PT or thermal event), one needs to question whether the system is acting inefficiently based on the expected event?
- **1st objective:** Determine the energy path of the unfocused distribution of states through particle entanglement measure. Then, reroute the energy path by focusing its distribution through lenses. This satisfies a desired Hamiltonian from particles contributing to an efficient system performance.
- **2nd objective:** Satisfy the 1st objective by recording and separating (labelling) particle energy states into groups of ground states (GS) and excited states (ES). The recording is when the CNOT operator acts on the input state in a qubit register as an adder Hamiltonian.

The register consists of at least one trapped *slave particle* with a *slave Ising spin* [28,29]. This involves the pairing of the fermion operators to a boson field Φ , as \mathbf{k} -based. An atom's spin flip by a CNOT operator operating on the QDF is counted by the slave boson. Definition 2 below, defines the QDF transform from [4] via [9,10].

System measurement requirement

The following method definitions and equations construct and evaluate system model boundaries as the thermodynamic limit [1], relative to quantum operations describing PTs via a QDF transformation observed in the system. This satisfies the requirement for achieving reliable measurement outcomes, such as achieving the desired Hamiltonian from the method's 1st objective based on a QDF circuit operation in the system.

Method definitions and equations

In lower Fig. 1, the simulated photoprobes by DFC, measure particles' average momentum $\langle \mathbf{k} \rangle \rightarrow 0$ as small (a long wavelength or red shift) and read a large value $\langle \mathbf{k} \rangle \rightarrow \infty$ (a short wavelength or blue shift) as they exchange energies between the opposing thermal sides of the system. The photon in the probe's field is detected by a photodetector, as its \mathbf{k} -based readout can provide information about a desired Hamiltonian from an expected measurement, e.g., which particle state is needed to be measured from a focused distribution of that state?

The following definitions followed by equations from [4,6] are key to implement the model and its algorithm.

Definition 1. An event is defined as an ST, like a particle *spin transition* (flip) on a magnitude of $|j|$ event occurrences (event frequency) that contributes to a PT, where j is the particle's j -th state. To determine a classical PT (CPT) or a QPT, the system's *thermodynamic elements* need to be *measured* using photoprobes and photodetectors to record system events as a lens coding technique.

Definition 2. A scalar QDF is a field where its spatial dimensions are doubled by a pairwise field scalar operation. This operation collapses the field to its pair with an ST probability of $P(\Psi \leftrightarrow \Phi) = |\langle \Psi \Phi \rangle|^2 \ni \langle \mathbf{k} \mathbf{r} \rangle$, where $\langle \Psi \Phi \rangle$ is the QDF correlation function. The field dimensions cancel out, if via κ , \mathbf{k} and \mathbf{r} correlate as $|\mathbf{k} \mathbf{r}| \rightarrow 1$. This is satisfied by a photoprobe state projection onto a pairwise particle state [4].

The measurement steps for the thermodynamic elements can be simulated by DFC applying the following operations [6] for each element:

1. Measure particle (average) momentum relative to position, or, equivalently, frequency [30].
2. Measure the expected correlation $\langle \mathbf{k} \mathbf{r} \rangle$ in $\langle \Psi \Phi \rangle$ as particles pair up from their sites within or between systems A and B as a QDF. Site l has a particle in state i . A neighboring site l' with a probability to have a particle, can pair up and entangle with the particle in site l , as described by quantum state $|i_{ll'}\rangle$.
3. Measure the statistical distance in qubits by defining EE, [18,23,24], between the quantum lens products generated from particle sites in systems A and B .
4. Apply CNOT to the sites for recording particle states toward the final state of the system.
5. Measure EE, where a CPT or a QPT is determined from the encoded entangled states between a sampled particle in B , paired with a particle in A , i.e., from the entanglement detection area in Figs. 1(a, d).

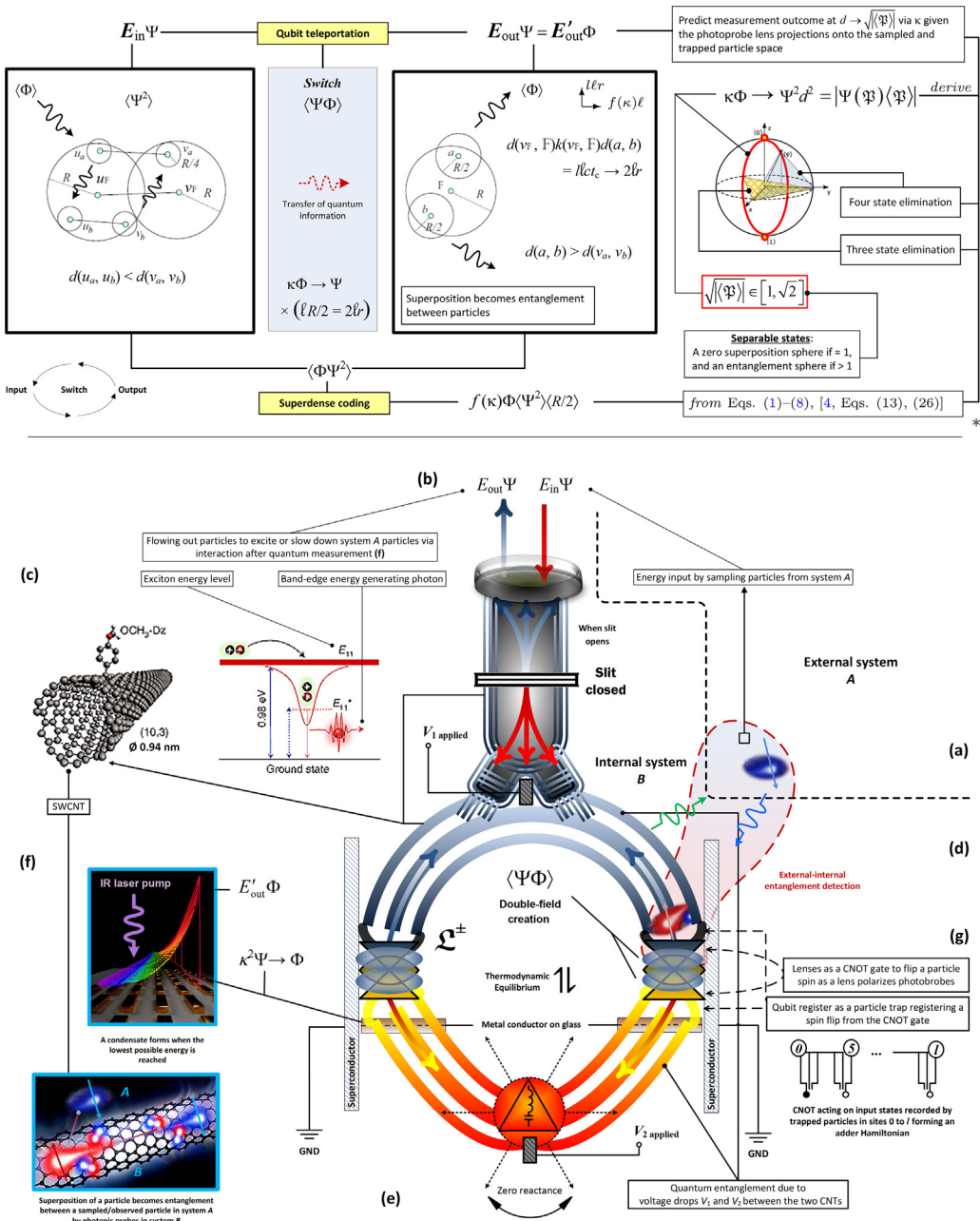


Fig. 1. DFC for a thermodynamic model: (a, b) Measurements are done within the internal system *B* after sampling particles from external system *A*. (c) Photons are generated in a SWCNT as photoprobes to conduct measurements. (a, d) External-internal entanglement is detected between particles in *A* and *B*. (e) A PT and entanglement are observed via superconductivity relative to voltage drop and application. (f) Superposing particles entangle where photoprobes are detected by photodetectors. A measurement readout from an entangled pair is their entanglement scaled between two or more QDF points, Eq. (6). (g) Lenses function as a CNOT gate to (dis)entangle particles relative to (d)–(f) events contributing to a QPT. An adder Hamiltonian is formed by trapping particles that record which CNOT operator acted on the input state. The black dot is one of the CNOT operators that has acted on a 3-qubit input, while others remain in state $|0\rangle$. The count is to measure how many times entanglement has occurred. * Upper figure: A theoretical framework according to the QDF model proposed by [4] via [9,55,56], corresponding to the lower figure and Fig. 2 events. The model focuses on particle pairing, entanglement and the predictions of states under a QDF transformation.

The correlation between the output, the PT switch as the magnetic slit in Fig. 1, and the input in Eq. (11) can be determined by measuring the ST probability of the field transformation. The magnetic slit opens and particles from system A are sampled in system B , given their energy states. This is where a PT switch is turned on for a thermal event. This measurement is from a distance between two field points, a and b ,

$$\lim_{|\mathbf{kr}| \rightarrow 1} d(a, b)\ell |\mathbf{kr}| = d(v_F, \mathbb{F})k(v_F, \mathbb{F})d(a, b) \rightarrow d(a, b)\ell = \ell R/2 = 2\ell r \leq l\ell c t_c, \quad (1)$$

where a PT decays over time t_c with some probability, Eq. (2), as $ct_c \rightarrow \lambda_c$ after a κ operation, and $d(v_F, \mathbb{F})k(v_F, \mathbb{F}) = |\mathbf{kr}|$. This measure, for example, is required in the QDF system to determine the state and position of a quantum particle as a hidden prize, which is the target state (TS) of a particle interacting with the prize expecting to win in a QDF game [4, Sec. 1 and Appx. A]. This is measured relative to any other quantum particle interaction during a QDF operation. The prize is prepared by Alice in a quantum state as her TS, hidden from Bob in a box among a set of boxes or traps (out of three), so that Bob is given the choice to choose (switch to) a box with or without the prize [4]. Bob can win the prize as his TS against Alice's TS who expects Bob not to win as her prize. In this system, Alice, Bob and the prize, are particles who can change roles within their associated fields (of receiving or emitting photons) according to their chosen quantum measurement and readout points [4, Sec. 2.2]. The roles of these game participants are listed in Meth. Valid. I, p. 16.

Given the least uncertainty bound discussed in [4, Sec. 4], and $\min l = 4$ from Example 2, the quantum information exchange with some probability P between two field points, a and b , is

$$\min l r P_{ab}/2P_{ba} \xrightarrow[\text{switch}]{\kappa\text{-field}} 4\mathbf{r}_{i,j} |\langle f(\kappa)\ell' \rangle| = \langle R/2 \rangle, \quad (2)$$

where $r = |\mathbf{r}|$, and $\{\mathcal{P}_{ab}/\mathcal{P}_{ba}\} \rightarrow |\langle f(\kappa)\ell' \rangle|$ describes a PT into a QPT or CPT as it decays over time t_c .

The correlation between \mathbf{k} and \mathbf{r} is measured by the QDF correlation function $\langle \Psi \Phi \rangle$. From this measurement, the quantum state of particles can be determined as the correlation length λ_c diverges at a critical point (a PT) [15,16], which can scale to λ_p [4], for a QPT. The measurement is conducted wherever the QDF is formed, such as particle pairing [28] at the lenses (a combination of concave and convex lens functions).

The energy path creation, or the decision to reroute particle states from a disordered state of system A , in system B , is done by determining the superposition and entanglement between a set of fast and slow particles that have a net spin-up GS, as in the ferromagnetic case [25], Fig. 3(c). The paired particles are counted by

$$\mu_{ij} = (N^2 - N)/2, \quad (3)$$

which is the number of pairwise particle interactions exchanging energy between sites i and i' . This energy exchange contributes to a QDF lensing event caused by a quantum lens which creates the i th and j th events between the two sites. These events are STs based on pairwise spin flips. The interaction length between particles via κ , scales to μ_{ij} counted within L , as $L \rightarrow \lceil L\mu_{ij} \rceil$. The number of particles entangled in the range of L scaling to L_ε , is counted by the adder Hamiltonian relative to lens distance d defined in Eq. (9),

$$\mu_d = \lim_{L \rightarrow [0,1]L_\varepsilon} \lceil L\mu_{ij}/Nd \rceil. \quad (4)$$

For the minimally entangled particles, L tends to $L_\varepsilon \approx 0$. The particle states entangled between sites i and i' have wavevectors $\mathbf{k}_{i_{ll'}}$ and $\mathbf{k}_{j_{ll'}}$, and positions $\mathbf{r}_{i_{ll'}}$ and $\mathbf{r}_{j_{ll'}}$, where $|\langle \mathbf{k}_{i,j} \rangle_{ll'}| = |\mathbf{k}_{i_{ll'}} - \mathbf{k}_{j_{ll'}}|$ and $|\langle \mathbf{r}_{i,j} \rangle_{ll'}| = |\mathbf{r}_{i_{ll'}} - \mathbf{r}_{j_{ll'}}|$. The non-entangled states have wavevectors \mathbf{k}_i and \mathbf{k}_j , and positions \mathbf{r}_i and \mathbf{r}_j , [4, Sec. 4]. The magnitudes of the expected position product $\langle \mathfrak{P} \rangle$ and wavevector product $\langle \mathfrak{K} \rangle$, are respectively

$$|\langle \mathfrak{P} \rangle| = \left| \langle \mathbf{r}_{i_{ll'}} \mathbf{r}_{j_{ll'}} \rangle \right| \quad \text{and} \quad |\langle \mathfrak{K} \rangle| = \left| \langle \mathbf{k}_{i_{ll'}} \mathbf{k}_{j_{ll'}} \rangle \right|, \quad (5)$$

given that entanglement is always contained in the QDF, mainly in form of these products. This is frequently encountered in Method. Valid. I, corresponding to Fig. 1 events.

The information transmission from the QDF over a quantum channel via κ is satisfied by measuring the photoprobe's momentum off of a particle pair. The photoprobe-particle pair interaction increases or lowers the probe's energy state. This denotes a momentum transfer from the pair to the photoprobe, as $|\mathbf{kr}| \rightarrow 1$. The particles' physical information is collected by the probe on a magnitude of $|\mathbf{r}|$:

$$\kappa^2 \Psi = \kappa^2 \sqrt{N\rho(\mathbf{r})} e^{i\mathbf{k}_{i,j}\mathbf{r}} = \kappa^2 \psi_{i_n}(\mathbf{r}) \rightarrow \phi_{i_n}(\mathbf{k}) e^{i\mathbf{kr}} = \Phi, \quad (6)$$

where i is the imaginary unit, and state i_n corresponds to the n th particle which assumes state i in its site, and ρ determines the probability (density) that the particle in state i will be found at position \mathbf{r} , via $\mathbf{k}_{i,j}$, Eq. (5). The transformation is "reciprocal" via a κ^{-2} -operation, given the convergence for that n th particle by pairing it with other particles to gather information about \mathbf{r} . The ES $|i\rangle = |1\rangle$ can be determined by its scattering factor $e^{i\mathbf{k}_{i,j}\mathbf{r}}$ through the photoprobe's field Φ . The GS $|i\rangle = |0\rangle$ can be determined by the condensate density $\rho(\mathbf{r}) = |\Psi|^2$. This is achieved by observing STs, prior and after a PT, caused by a QDF switch, as discussed below.

The QDF transform has the following transition probability

$$\mathcal{P}(\Psi \leftrightarrow \Phi) = |\langle \Psi \Phi \rangle|^2 \sim |\langle \Psi(\lambda_p) | \Phi(\lambda_c^{-1}) \rangle|^2 \geq 1/2. \quad (7)$$

The QDF correlation function $\langle \Psi \Phi \rangle$ is equal to 1, if field component \mathbf{k} or \mathbf{r} multiplied by κ satisfies the conversion of $|\mathbf{kr}|$ to a constant $|\mathbf{k}|^2 = 1$. This is due to a planewave travelling along \mathbf{k} , which reciprocally satisfies a QDF transformation and its measurement outcome. From Eqs. (1)–(7), a field transformation constructing a QDF is

$$\kappa \Phi \rightarrow \kappa^{-2} \Phi \ell r = \Psi^2 d^2 = |\Psi(\mathbf{p})\langle \mathbf{p} \rangle|, \quad (8)$$

which denotes Φ transforms into Ψ via κ relative to λ_c and λ_p at sites l and l' .

As $|\mathbf{r}| \rightarrow \lambda_p$, $\lambda_c = |\kappa^4 \mathbf{r}^{-1}|$ diverges to ∞ at a critical point, [15,16]. The projection of an output state from Φ onto an input state from Ψ , gives the photoprobe a linear superposition with an ST probability $\geq \frac{1}{2}$. To determine the length divergence, the quantum lens distance d between two lensing events needs to be measured.

Definition 3. Lens function \mathfrak{L} as \mathfrak{L}^+ takes all particle states from sites l and l' , and gives 1 convex (focused) product of m -level j states with an $\mathbf{r}_{m;j_{ll'}}$ (super-)position. Len function \mathfrak{L} as \mathfrak{L}^- takes all particle states and returns a concave product of states with $\mathbf{r}_{i,j}$ positions. A mix of concave and convex products is a product of a convex-concave lens function \mathfrak{L}^\pm .

Definition 4.

- a) A lens product is the result of a *lens work*. The *work done* is the energy transfer from a lens to focus or defocus energy states for a particle, causing it to gain or lose momentum via a pairwise interaction. The work is done when a lens product is observed over a lens distance d relative to lengths λ_p and λ_c between fields Φ and Ψ of Eq. (7).
- b) The lenses *force* the photons that are generated from the external CNT layer to focus and defocus the distribution of particle states. This is achieved by projecting the photons onto a path of atoms based on correlation $\langle \Psi \Phi \rangle$ between their average momentum $\langle \mathbf{k} \rangle$ and average position $\langle \mathbf{r} \rangle$.
- c) The CNTs, lenses and magnetic field components as forces of *external* and *internal fields* (as in the Ising model [17,18,75]) affect particles to produce a GSM (ground state matter), as well as measuring the statistical distance between them.
- d) A series of GSM productions from a broad range of GSs can scale to the production of a BEC from a specific GS in a trap [4, Remark 8]. An entangled BEC EPR pair [59,61,62], created at a lens distance of d , each BEC of the pair is a lens product observed over a quantum communication channel relative to d .
- e) The distance for the quantum channel scales to entanglement length $L_\mathcal{E}$ between the entangled EPR pair, and is evaluated by Eq. (28) for any d between two lens products that can scale to $L_\mathcal{E}$ in a QDF circuit.

An example of a concave lens function \mathfrak{L}^- is that it can produce maximally entangled (two-qubit Bell) states in the system, Examples 1 and 4.B. This is achieved only when the experimental conditions of producing a GSM and its entanglement are met via e.g., convex lens coding. The measurement method is conducted on the periodic events of the system, as shown in Fig. 2. The expected lens distance for \mathfrak{L}^- to produce entangled states from Eq. (9), is short between BEC particles, and long when far and scattered through diffusion. Both outcomes can be satisfied by a sequence of convex-concave and concave-convex products. An example of a convex function \mathfrak{L}^+ is that in Fig. 2(a), up to N particles in one or more quadrants of the energy surface (of e.g., lattice sites) interact with a light beam projected from the convex lens, p. 2. Here, the beam projects onto the closed surface inside system B when the slit is closed, Fig. 1(b). This can produce BEC, and/or entangled EPR pairs within a QDF field, Figs. 1(g), 3(d), and Example 2. The combinational use of both lens functions, during and after particle sampling, continues to produce lens products in a periodic flow of thermal events between systems A and B , Fig. 2.

The lens distance as a function between two lens products via lensing events, STs and PTs, one as a micro-level, and the other as a macro-level observation within the system, is

$$d(\mathfrak{L}^-, \mathfrak{L}^+) = \left| \mathfrak{L}^-(N) \mathbf{r}_{i,j}^2 \lambda_c^{-1} - i \mathfrak{L}^+(N) \mathbf{r}_{m;j_{ll'}}^2 \lambda_p^{-1} \right|, \quad (9)$$

where the unit $i = t^{4n+1}$ is used to describe the photoprobe's field projecting photons onto the particle-pair space relative to the Planck length $\lambda_p \approx 10^{-35} \text{ m}$ [4], as the possible *quantum measurement point* [4, Sec. 2.2]. This is expressed by $|\mathbf{r}_m| \gtrsim \lambda_p$, which denotes a photon from its probe field travels at light speed c across a magnitude of Planck positions in the lattice, where a counter particle (trap) is formed as a GSM or BEC. Ground state modes of $m > 0$ are expected from this measurement for the GSM, see p. 11. The robe's field carries the frequency of a sampled particle from its pairwise site measured by $\langle ll' \rangle$, Eqs. (5), (16) and (21) in creating BEC pairs, see Example 2.B and Alice's role on pp. 13–16. From Eq. (5), $\mathbf{r}_{j_{ll'}}$ denotes particle entanglement in Eq. (9) for a correlated system, as an entangled BEC EPR pair. In the lattice QDF model, $\mathbf{r}_{j_{ll'}}$ alters to length L , scaling to $L_\mathcal{E}$ which scales as λ_c , and only diverges at a critical point where $|\mathbf{r}| \rightarrow 0$ and $\lambda_c \rightarrow \infty$, given Eq. (7).

A \mathbf{k} to \mathbf{r} -based field transformation from Eq. (7) has an ST probability

$$\mathcal{P}(\Phi \rightarrow \Psi) \approx 4(N-1)^2 / 9\theta_{ij}\mu_{ij} \geq 2/3, \quad (10)$$

where $\theta_{ij} \in [\frac{8}{9}, 1]$ is the pairwise particle adjustment factor adjusting the result against the irreducible $\frac{8}{9}$ produced for a big N , [4]. This probability is determined for N interacting particles sampled from an input state of a \mathbf{k} -based field Φ describing a photon, coupled with an output state of an \mathbf{r} -based field Ψ describing an atom, Eq. (9). The adjustment factor θ_{ij} is applied due to one particle of the pair *misbehaves* (uncontrolled) within the given interval $[\frac{8}{9}, 1]$. The trapped particle behaving within the range of the interval is superposing with ≈ 0.1 or 10% level of uncertainty, which is $\geq 90\%$ probability to be in position. Thus, an ST probability of $\mathcal{P}(\Phi \rightarrow \Psi) \approx 1$, is by projecting and coupling an input state with an output state, Fermi's golden rule [1], based on superposition between the free and trapped particles.

The converse of Eq. (10), $\mathcal{P}(\Psi \rightarrow \Phi)$ with the same range of probabilities is determined based on the sampled atoms for the input state, paired with an output state of a photoprobe for an atomic state readout.

A PT occurs from the QDF as a tensor product $|\psi\rangle \otimes |\phi\rangle$. Depending on the field intensity $\sim \lambda_c^{-2}$ resulting from photonic projections, field emissions cause a switch from one energy state to another

$$\underbrace{\langle\Psi|E_{in}|\Phi\rangle}_{\text{input}} \xrightarrow{\text{switch}} \underbrace{|E_{i_n}\langle\Psi|\Phi\rangle|}_{\text{phase transition}} \xrightarrow{\langle f(\kappa)\Delta E\ell\rangle} \underbrace{\langle E_{out}\rangle}_{\text{output}}, \quad (11)$$

where field Φ associates a scalar value by its switch function $f(\kappa)$ for an output state from ΔE , which is independent of a κ -based field transformation between energy states. The field Ψ via $f(\kappa)$, and λ_c satisfying the field intensity, result from a photon-atom projection which can form a direct sum $|\psi\rangle \oplus |\phi\rangle$ of the two fields Ψ and Φ , relative to the expected values of E_{in} and E_{out} . In the switching process, the expected energy output is lower than the energy input, $\langle E_{out}\rangle < E_{in}$, where $\langle E_{out}\rangle$ is useful to an n th sampled particle if it entangles with the trapped particle. This achieves an ES as a momentum transfer from the trapped to the sampled atom.

The switching operation via $f(\kappa)$ in Eq. (11) is

$$\Delta E = E_{i_n} - E_{i_m} = 2E_0|\Delta i|, \quad (12)$$

where $|\Delta i| = |i_m - i_n|$ is the magnitude between the input state and output state, E_0 is the zero-point energy of a quantum oscillator, e.g., a BEC trap in Figs. 1–3. The system's expected energy can be calculated from $|\Delta i|$, given i_m and i_n values, which determine i . Thus, $\langle E_{out}\rangle$ is predicted as the change $\Delta E\ell$ in a QPT, Eq. (11).

The value of $f(\kappa)$ in Eq. (11) can be determined relative to the 6 particle positions quantified in Eq. (10), with a ratio of $\alpha^2 = \{4k_{ij} : 2r_{ij}\}$. Their probability density function is $\rho = \rho(k_{ij})$ or $\rho(r_{ij})$, which ranges between the upper and lower bounds of the scalar, $|\kappa^2|\rho \leq 2$, [4]. The bounds of scalar κ rewrites the ST probability from Eq. (7) as

$$\mathcal{P}(\Phi \leftrightarrow \Psi) = f(\kappa)|\langle\Psi|\Phi\rangle|^2/2 = f(\kappa)\rho/2 \in [|\kappa^2\alpha|^{-2}, |\kappa^2\alpha|^2]/2 = (0, 1], \quad (13)$$

which can be used in a density matrix to determine N -particle entanglement generated from superposition. An ST probability $\geq 2/3$ denotes a QPT at λ_p , and denotes a CPT at a distance of $d \gg \lambda_p$, [4]. The code, based on a QDF lens operation, is comprised of qubits that represent the information about the transition between an input state and an output state, as well as their lens distance to determine an ST probability $\geq 2/3$, Eq. (10).

Definition 5. In a binomial trial [1], and from Definition 3, a lens output state o is observed after an ST with probability 1, which is a successful classical state (or a failed quantum state) outcome. The opposite outcome of any trial is a mixed output state. Its density matrix representation has a probability $p < 1$ for $|0\rangle$ or $|1\rangle$.

Definition 6. The entropy of the reduced density matrix ρ_A (equivalently ρ_B) is EE as $S(\Psi_{AB}) = S(\rho_A) = -\text{tr}(\rho_A \log \rho_A)$, which counts the number of entangled bits between systems A and B , where $\rho_A = \text{tr}_B \rho_{AB}$, and tr_B is the partial trace of a pure or a mixed system state ρ_{AB} . For a pure state, $\rho_{AB} = |\Psi\rangle\langle\Psi|_{AB}$, and $S(\Psi_{AB}) = S(\rho_A) = S(\rho_B)$, where $|\Psi\rangle_{AB} = |\Psi\rangle_A \otimes |\Psi\rangle_B$ is a joint state (e.g., the joint state of two photons is pure [18]).

From Ref. [6], the following examples use the definitions above in formulating the QDF algorithm from the DFC model on p. 9:

Example 1. If systems A and B each have n qubits, then in a maximally entangled state, $S(\rho_A) = n \log 2$. $S(\rho_A)$ counts the number of bits, or $e^{S(\rho_A)}$ counts the number of entangled states (since n qubits have 2^n states) [12,24]. The entanglement contained in $|\Psi_{AB}\rangle$ between A and B is measured by $S(\Psi_{AB})$. This is used as the quantum information to create or reroute energy paths for a set of particles not participating in a thermal event.

Example 2.A. A light source emits random polarized photons through a lens as a polarizing beam splitter, which changes the path of a photon if its polarization is in a polarization state flipping an atom's spin. This is a control qubit forming a CNOT gate, and the target qubit is the path of the same photon hitting the atom [38]. The density matrix for the state of photons is $\rho = |\phi\rangle\langle\phi|$. For each step of polarizing the photons horizontally (control qubit) with an up path (target qubit) state $|0\rangle$, or vertically with a down path state $|1\rangle$, ρ 's index is incremented by 1. The density matrix for the emission is $\rho_1 = \frac{1}{2}|0\rangle\langle 0| + \frac{1}{2}|1\rangle\langle 1| = \begin{bmatrix} 0.5 & 0 \\ 0 & 0.5 \end{bmatrix}$. From Definition 5, the lens output $o = \text{tr}(\rho_1^2) = 0.5$ is observed as a mixed state. If a second lens function as a CNOT gate is applied, a vertical plane polarizer disentangles the photons. The lens output is $o = \text{tr}(\rho_1^2 \rightarrow \rho_2) = 1$ which is scaled up to the maximum value of scalar κ for the pair, $|\alpha^2|^2 \rightarrow 2$, Eqs. (6)–(9). This achieves a pure state expressed by a density matrix $\rho_2 = d|\kappa^2\alpha|^{-2} = 2\mathfrak{L}^+ \rho_1 = L_E \begin{bmatrix} 1 & 0 \\ 0 & 0 \end{bmatrix} \begin{bmatrix} 0.5 & 0 \\ 0 & 0.5 \end{bmatrix} \approx 2 \begin{bmatrix} 0.5 & 0 \\ 0 & 0 \end{bmatrix}$. This result is obtained due to the maximum distance scaled to L_E between the paired photons. The polarization is done twice as two lensing events, with an event frequency (Definition 1) of $|j|^2 = (2\text{nd and 3rd ST}) = 2$, to fully polarize the mixed state. The final event is a pure vertical state at the maximum length scale of entanglement, which is detected by the photodetector. The atom's state is recorded with probability 1, denoting zero entropy.

From Refs. [6,59,61,62] and Definitions 4c) and d), Example 2.A can be expanded to the following example:

Example 2.B. From Example 2.A, photonic entanglement can be prepared by a beam splitter operation [61]. In Figs. 1(f, g), this beam splitter is provided by the QDF lenses and its interaction with particles is between the lenses and the metal conductor where lasing and BEC are produced. Among the sampled particles in system B , BEC is produced in a trap, Figs. 1 and 3(d). The beam splitter

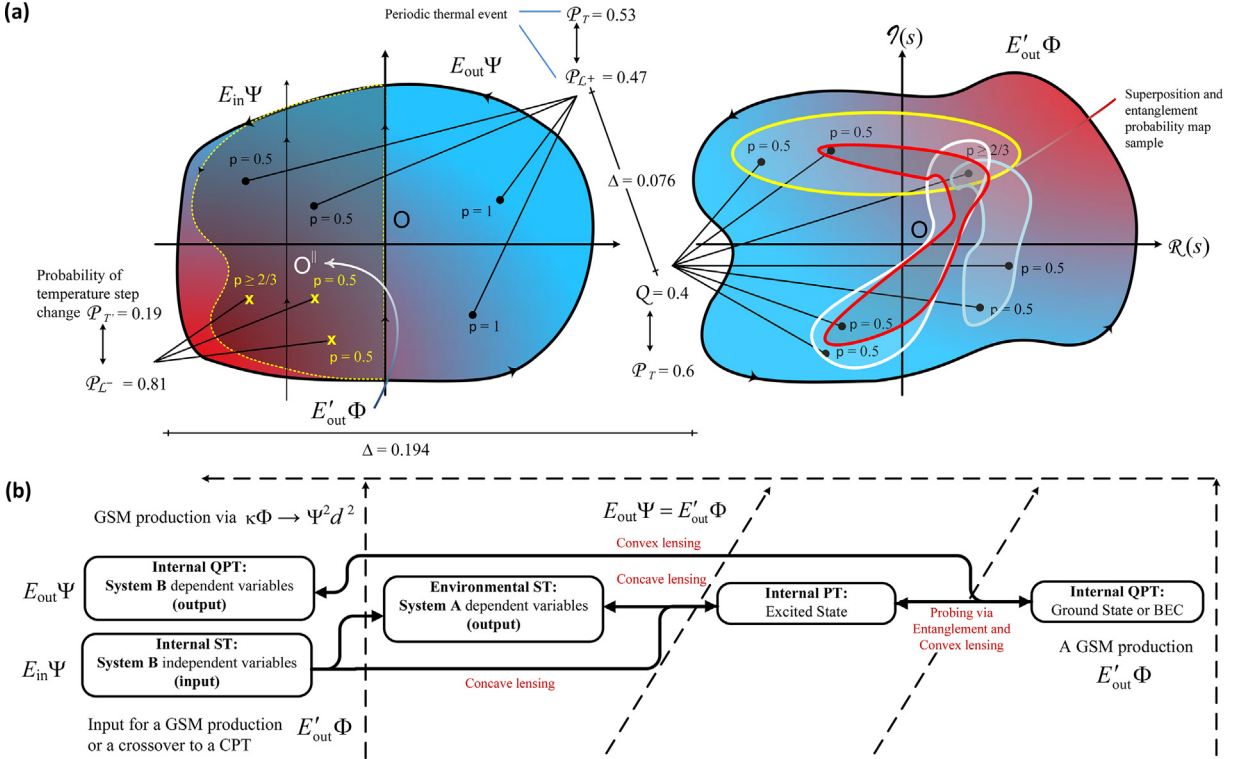


Fig. 2. (a) A DFC example to simulate a lens input-output product from the proposed system, Fig. 1. Internal system *B* (leftmost) equipped with lenses, after sampling from the external system *A* (right-to-left), projects and distributes particle states. This is shown by a particle superposing between the input side and output side, with a $p = .5$. A GSM or BEC production is shown as a QPT against an internal PT in *B* (left-to-right). (b) The periodic thermal event flow (system energy path, 1st objective on p. 3) maps the p 's of a spin flipping event in \mathcal{O}^{\parallel} to \mathcal{O} via entanglement, and to convex coding areas between the p 's within the quadrants. The dotted arrows cover and point to the quadrants where the flow carries the expected lens products relative to a temperature step. The flow direction favours the expected system state in (a). (a, b) Each quadrant has a probability sum of 1 over one or more events as the magnitude of their occurrence (frequency), Eq. (23). This probability sum falls on the same axes' side. The coding areas for a greater magnitude of events across the quadrants denote superposition or entanglement, and have different colors to distinguish between system temperature steps by measuring probabilities P_T and $P_{T'}$, Table 1. The shared value of $p \geq \frac{2}{3}$ is distributed in system *B*, given the ST probability $P(\Phi \rightarrow \Psi) \geq \frac{2}{3}$ via κ , which indicates superposition and entanglement between particles in *A* and *B*. The information about the possibility of entanglement is extracted from the counter particles in *B*, with slave Ising spins.

operation is applied on single mode squeezed states generating a two-mode squeezed state as two spatially separated BECs from a BEC in two traps [61,62]. This corresponds to an entangling Hamiltonian between l and l' in the system with a spin-spin Bell state correlation, see Eq. (17). This is the entanglement between BECs produced by splitting a single squeezed BEC into two spatially separated BECs. Alice via the box, as an EPR pair, can represent the sum of Bell correlations up to $(4/\sqrt{2}) = 2\sqrt{2}$ from the four possible combinations of Bell states $|ij\rangle_{ll'} = |\{00, 01, 10, 11\}\rangle_{ll'}$. The pair can perform a quantum teleportation, e.g., Alice as the sender of the qubit information on the prize state to a box as the receiver. The box with the prize can teleport its state to another box. Alice and the box resource, which is the prize state, is shared as the EPR state with Bell correlations observed within a BEC, and between the EPR pair [62]. Alice mixes her input state with her EPR state at the beam splitter which can function as a CNOT gate, Example 2.A. Alice then sends the qubits through the CNOT gate, and the first qubit through a Hadamard gate. Alice performs a Bell measurement on her qubits obtaining one of the four Bell state results, and sends the classical result (two classical bits) to the box. The box from this classical result performs a phase-space displacement on its GS mode (half of the EPR pair) to recover the original unknown input state and change or unchange the prize state. The prize state remains entangled with Alice, or becomes (transitioned into) a GSM or a BEC in one of the boxes. This teleportation can be performed between the pair through the QDF compatible components: QFT and QFT^{-1} which implement the interaction potential and kinetic energy operators on states $|i_{ll'}\rangle$ and $|j_{ll'}\rangle$, see EE encoding, Eqs. (29)–(35). The same QDF components are used to perform the inverse of teleportation as superdense coding to decode the EPR state in the QDF circuit, upper Figs. 1 and 5. Other parties e.g., Eve can share the EPR state from the entangled pair with Bob to see which box is with the prize.

As discussed in [4, Sec. 2.2.], the roles of these participants can change as quantum measurement points and readout points in the QDF circuit. The QDF for the k and r transformation between the BEC pair field is associated to the beam's field where Alice is entangled. Here, the scalar κ is applied to the spatial dimensions where k and r correlate as $|kr| \rightarrow 1$ in the QDF. If a third party, like

Eve, have her state as a qubit mixed with the entangled Bell states, all measurement outcomes from the output are distinguishable states, Eqs. (25)–(27).

Method algorithms

System model boundaries, as defined and discussed in the last section establish the DFC algorithms from [6], which satisfy method's 2nd objective followed by EE measurement to simulate the thermodynamic system.

Model boundaries

The following sections from [4,6] are key to determine EE between systems A and B from the QDF circuit.

Steps of the QDF modelling cycle

Fig. 2(b) shows the steps of the QDF modelling cycle corresponding to the thermodynamic events of Fig. 2(a). The flow starts from the left side of the contour to the right, and cycles back from there.

Steps of the QDF algorithm

Entanglement is observed from an N -body quantum state $|\psi\rangle$ between systems A and B , Figs. 1(a, d). This requires presenting the QF-LCA's structure in our method before executing it on an N -qubit machine.

From one EE measurement to another in a PT loop, the N -body state is encoded into a product state of a Schrödinger's cat state (in short, a cat state) [12,13,39]. The encoding is implemented by *superdense coding* [40,64–66] between particle pairs, step 3 of Algorithm 2, after sharing their entangled EPR state from teleportation, step 2 of Algorithm 2. To satisfy this process, steps 1(a)–(b) of Algorithm 2 need to be implemented. In those steps, the control qubit in the CNOT operation is a photoprobe that can flip the state of an atom to disentangle or entangle the atom (due to $h > 0$) with another atom. This is performed via particle spin-spin or spin-squared interaction between two lattice sites, or traps in case of BEC EPR pair creation, Example 2.B. This CNOT operation includes producing BEC (a GSM) from a classical state, using the same photoprobes that target an atom's spin to flip [3,7].

Algorithm 1: DFC of entanglement entropy and system efficiency.

Require: Use the N -body quantum state based on the Hamiltonian H from Eq. (16).

Ensure: Construct the corresponding reduced density matrix $\rho = |\psi\rangle\langle\psi|$ as the output.

- 1: Define the inside area of system B . The outside environment of B is system A area where particles are sampled and traced out of the density matrix: $\rho_B = \text{tr}_A \rho$.

- 2: Use the reduced density matrix to compute EE:

$$S(\rho_B) = -\text{tr}(\rho_B \log \rho_B) = -\text{tr}(\rho_A \log \rho_A) = S(\rho_A). \quad (14)$$

- 3: The initial state is maximally entangled if $S(\rho_B) = \log 2$, and not entangled if $S(\rho_B) = 0$, [26, 40].

- 4: Maximize system efficiency in determining the scalar behaviour of entanglement (discussed in EE scaling and Eq. (16)) by a κ -based QDF transformation and doubling the ST probability in the density matrix (see Remark 5).
-

The EE measurement choice

Fig. 3(b) shows λ_c for non-critical phenomena translating to a finite entanglement length L_E . This length has a value of L for which adding new spins to a block does not increase its entanglement with the rest of the chain. As in the Ising model [18–20,75], L_E diverges at the critical point $h = 1$, which is when $|\mathbf{r}| \rightarrow \lambda_p$ and $\lambda_c \rightarrow \infty$ in Eq. (7). As $h > 0$ (yet, $h < 1$), the GS products $|0 \dots 0\rangle$ and $|1 \dots 1\rangle$, given $|1, m\rangle = |0, m-1\rangle$ for $m > 0$ modes, are not fully degenerate due to a splitting of order h^N between the products $|\Psi\rangle_{AB} = \frac{1}{\sqrt{2}}(|0 \dots 0\rangle + |1 \dots 1\rangle)$.

The following example shows the coding model for determining entanglement in a periodic quantum compression and decompression of particle states [6,71].

Example 3.B. The inside area of system B , Fig. 2(a), is the particle site. This area is partitioned into four observable quadrants (as in the unit circle) of energy surface \mathcal{O} , spanning from the energy input phase $E_{\text{in}}\Psi(t)$ to the energy output phase $E_{\text{out}}\Psi(\tau)$. In the classical case, the input states are given in four observable quadrants of energy surface $\mathcal{O}_{q \leq 4} = \{\mathcal{O}_1, \mathcal{O}_2, \mathcal{O}_3, \mathcal{O}_4\}$ in systems A and B . The inside area sites of parallel quadrants of energy surface $\mathcal{O}_{q \leq 4}^{\parallel} = \{\mathcal{O}_1^{\parallel}, \mathcal{O}_2^{\parallel}, \mathcal{O}_3^{\parallel}, \mathcal{O}_4^{\parallel}\}$ as quantum, Fig. 2(a) left, in B , can map to inside area sites 2 and 3 of \mathcal{O} via the photoprobe field Φ , Fig. 2(a) right, corresponding to the Fig. 2(b) flow diagram. This is defined as $|\Psi(t)\rangle_{\mathcal{O}} \xrightarrow{|\Phi\rangle} |\mathbf{1} \boxed{11} \mathbf{1}\rangle$ with the inside area sites 2 and 3 outlined (boxed) in the center, and outside area as sites 1 and 4. The density

Algorithm 2: DF lens coding of an N -body quantum state as a product state of classical and cat states.

Require: Input a qubit pair.

Ensure: Implement CNOT or CCNOT gates [65,37] and record their input and output. Decode qubits as classical bits by the recipient.

- 1: Implement a CNOT gate and encode classical data into qubits (consistent with IBM Qiskit convention [64,5])
 - (a) CNOT logic: *input the qubit pair → if the first (most significant or leftmost) qubit (control qubit) is |1⟩, then the cnot gate flips the second (least significant or rightmost) qubit (target qubit).*
 - (b) Encode a bit-pair denoting A and B system state using one qubit, compress and classically record (register) the compression of any qubit sequence based on CNOT logic: $|00 \rightarrow 00\rangle \in |0\rangle$, $|01 \rightarrow 01\rangle \in |1\rangle$, $|11 \rightarrow 10\rangle \in |2\rangle$, and $|10 \rightarrow 11\rangle \in |2 \rightarrow 1\rangle$. The last qubit compression $|2 \rightarrow 1\rangle$ in decimal is obtained through an IF-statement involving subtraction between the registered classical bits as $\underline{b}(11 - 10) = 3 - 2 = 1$, see Meth. Valid. I code examples.
 - (c) Assign the result as a new label number (data point), see Meth. Valid. II.
- 2: Keep a record (a qubit by a bit-pair as in *teleportation* [64,12,61,63,32], i.e., the opposite of superdense coding) on which CNOT gate denoted by $\mathbf{C}_{0 < s}$ operators operated on the input [37], where s is a step counted from a stepwise interval Δt^* . This is implemented by forming an adder Hamiltonian between the CNT layer and the lenses.
 - (a) Start counting by the adder with register qubits in the input state $E_{\text{in}}|\Psi\rangle$, and a counter particle (trapped) $\mathbf{c}_{0 \leq l \leq \mu_d}^\dagger$, based on Eq. (4) satisfying Fig. 1(g), at site $l = 0$. This counting occurs in real time $t = -i\tau$, where τ is the imaginary time. If the program counter particle is at site l , then the active CNOT operator \mathbf{C}_l flipping a spin is at $|0 \dots \underbrace{1}_{l} \dots 0\rangle \mathbf{C}_l \dots E_{\text{in}}|\Psi(t)\rangle$.
 - (b) If the particles' final state in B contains a Hamiltonian component with the counter particle at site $l \rightarrow \mu_d$, then the counting is finished. The rate to store the counted spin flips measured in Hz between sites l and l' , is $v_{ll'}$. The desired Hamiltonian after $\Delta t^* = tv_{ll'} - s$ steps, as a phase shift parameter, where $tv_{ll'} = t^*$, is projected out as

$$E_{\text{out}}^s |0\dots01\rangle\Psi(\tau) = \mathbf{C}_{\mu_d} \mathbf{C}_{\mu_d-1} \dots \mathbf{C}_1 E_{\text{in}}^{\Delta t^*} |\Psi(t)\rangle = \mathbf{c}_{\mu_d}^\dagger \mathbf{c}_{\mu_d} e^{-\beta_\tau E} |10\dots0\rangle\Psi(t), \quad s \in \mathbb{Z}^+, \quad (15)$$
 where the number of counter particles is a constant $\sum_{l=0}^{\mu_d} \mathbf{c}_l^\dagger \mathbf{c}_l$, \mathbf{c} is an untrapped particle, and $\beta_\tau = \tau/\hbar$ is the length of the τ interval [37,33,34], where \hbar is the reduced Planck constant. Also see Eq. (16).
- 3: Decompress gradually from the degenerate ground states in the superdense code to classical states using a combination of our system communication model, Ionicioiu and Wang *et al.*'s models [37,38,39,40].
 - (a) The compressed code is based on the cat state method, e.g. [39,61], and pairwise site BEC atoms with a product state from step 1(a), or see Example 4.
 - (b) The compressed quantum code can be decoded to classical bits by implementing CNOT logic [37]. All outputs are reversible to a set of classical or quantum states by inspecting the input states and the CNOT output using a photoprobe (see code listing examples).

matrix is $\rho = |1\boxed{1}\boxed{1}\rangle\langle 1\boxed{1}\boxed{1}|$. Hence, $\rho_B = \langle 0|_1\langle 0|_4\rho|0\rangle_1|0\rangle_4 + \langle 1|_1\langle 1|_4\rho|1\rangle_1|1\rangle_4 = |11\rangle_{23}\langle 11|_{23}$, and $S(\rho_B) = -\text{tr}(|11\rangle\langle 11| \log |11\rangle\langle 11|) = -\text{tr} 1 \log(1) = 0$. This corresponds to Fig. 2(b) as an internal ST → CPT occurrence in system B with probability 1 as a non-entangled state. In the quantum case, the area covers $E_{\text{in}}|\Psi\rangle$ in all parallel quadrants of $\mathcal{O}_q^{\parallel}$ returning $E'_{\text{out}}|\Phi\rangle$. From Definition 6 and Algorithm 1 steps 2–4, $|\Psi\rangle_{AB} = \frac{1}{\sqrt{2}}(|1\boxed{1}\boxed{1}\rangle + |0\boxed{0}\boxed{0}\rangle)$. Thus, $\rho_B = \text{tr}_A \rho = \frac{1}{2}(|11\rangle_{23}\langle 11|_{23} + |00\rangle_{23}\langle 00|_{23}) = \frac{1}{2}\begin{bmatrix} 1 & 0 \\ 0 & 1 \end{bmatrix}$ with entropy $S(\rho_B) = \log 2$ denotes a maximally entangled state.

In Example 3.B, for a number of photoprobes encoding $2n$ states (or n qubits) due to particle pairwising, Eqs. (3)–(8), there is at least one pair entangled, and a photoprobe superposed. Thus, maximum entanglement is observed between particles with entropy $S(\rho_B) = S(\rho_A) = n \log 2$ (Example 1). In this case, a cat state [12] is the most probable outcome as $h \in (0, 1]$, which is the external magnetic strength between the inside area sites of quadrants 2 and 3 entangled with area sites 1 and 4. This is subject to EE scaling, as follows.

EE scaling

1. Apply a 1D Ising model to the external CNT by having the Hamiltonian to compute EE, and see if any particles in A and B are entangled.
2. Apply a 2D Ising model to D -dimensional sites from e.g., the CNT interior for determining entanglement using photoprobes from the Φ field. Scalar κ transforms the field to a Ψ field for accurate readouts of atomic states. The prediction of spin flips to determine the system state is based on the thermal event probability from Table 1, to determine a spin flip from Eq. (15).

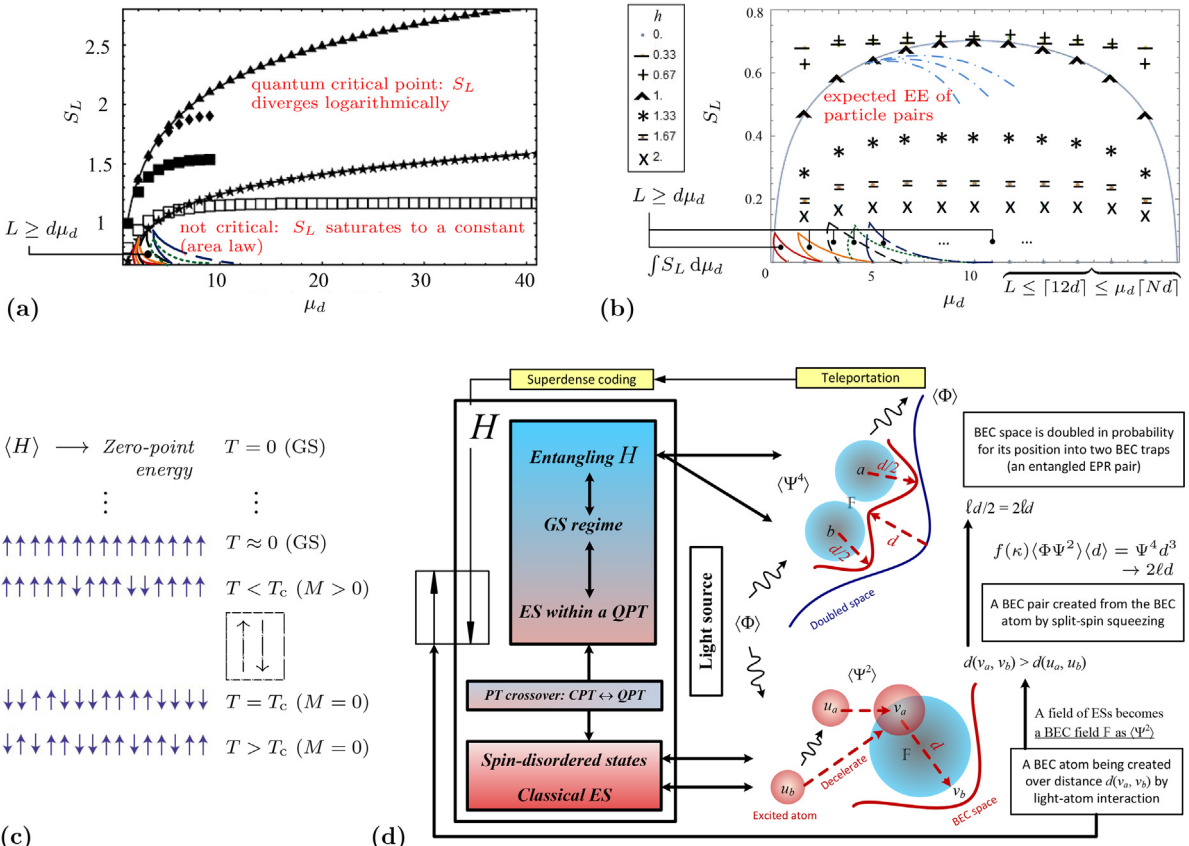


Fig. 3. (a) A noncritical Ising chain (\square) is with $J = 1$, and $h = 1$; noncritical chain (\blacksquare), has $h = 0$. A critical chain (\star) has a log divergence for a large $L \leq \mu_d [Nd]$, Eq. (4): $S_L \sim \log(L)/6$; the curve $S_L \sim \log(L)/3$ (\blacktriangle) corresponds to the critical chain with $h = \infty$, and $J = 0$. A chain of $N = 20$ spins (\blacklozenge) with zero magnetic field, combines critical log behavior, or low L , with a finite chain saturation effect, asymptotically described by a free boson [16–18]. (b) Given the QDF transform, non-entangled states conform to the point of entanglement, as entropy is measured for $L \rightarrow [10d]$, and decays as $N \rightarrow \infty$, i.e., the conformal field theory predicting 2nd and 3rd order PTs (of $D > 2$) [21,22]. (a) or (b) Sawtooth curves of $L \in [d\mu_d, \mu_d/Nd]$) form the area under the S_L curve by its integral, accounting for EE scaling based on pairwise interactions relative to a lens product delivered to a photoprobe at d . (c) Spin ordering simulation for the Ising model, as temperature increases (top to bottom) magnetization M changes to a zero net value. The correlation length increases when temperature is decreased (ordered spins), and diverges at critical temperature T_c . If the external field is absent ($h = 0$), there is still $M = 0$, [12,16,19,30]. (d) The cyclic production of BEC via atom-light interactions with an expected spin order in (c), to create BEC EPR pairs in an entangling Hamiltonian Eq. (17), scaled from H in Eq. (16), from an ES to a GS regime. Their space in probability doubles in a correlated QDF, Eqs. (1)–(8), as opposed to a disordered non-BEC space. Teleportation is performed after doubling, and the classical states are decoded by sharing EPR states via superdense coding.

3. Write a quantum code based on the coding steps in [Algorithm 2](#) and [Example 3.B](#), satisfying qubit compression and decompression. A classical state is extracted from the cat state based on the last two step predictions from a photoprobe readout. Entanglement with an expected probability ≈ 1 is extracted from the readout prior to its occurrence per spin flip.
- ⊗ The cat state is a macroscopic superposition of two ground states which gives an extra entanglement of $\log 2$. The field strength is $h < 1$, and $h > 0$ denotes a greater entanglement against a perfect entanglement on a scale of $h = 1$. For $h = 0$ and $h = \infty$, the GS is either the product state $|0 \dots 0\rangle$, or $|\uparrow \dots \uparrow\rangle$, denoting zero entropy. This is shown in Figs. 3(a, b) as an expected event between the SWCNT and the CNT interior, [Figs. 1\(d, f\)](#).
- ⊗ The input denoting entanglement is a black dot in [Fig. 1\(g\)](#), and the rest of the gates are the inverse (no entanglement or white dots). The photopropes are later used to decompress the count by reading the state of the trapped particles into classical states. Classical states during quantum decoherence are obtained by a gradual diffusion of BEC at a QPT level.
4. Distinguish and classify Bell states based on Eqs. (25)–(35) by using an extra physical qubits in [Fig. 1\(g\)](#).
5. Correct any possible qubit flip errors or information loss due to decoherence with the environment by [Fig. 1\(g\)](#) components. The components can encode any product states into an entangled state of $3[n, 2n \leq N]$ physical qubits from Eq. (32) to correct the qubit error [4,37], or see p. 20.

Remark 1. Quantum encoding, decoding and compression can be implemented on N -qubit machines, satisfying the computations required to perform the boundary conditions above, as a QDF circuit.

The Hamiltonian, EE, and energy conditions

The following Hamiltonian with EE scaling discusses the energy conditions for a desired Hamiltonian by the QF-LCA. This is to validate QF-LCA's products using QDF lenses and their measurement outcome.

The Hamiltonian with EE scaling

Consider N atoms occupy a 2D-array of L^2 lattice sites. Its entropy $S_L = S(L)$ is measured by observing any exceptions to EE's area law [30, Appdx. F], which holds for all gapped ground states on a 1D lattice [26,27,74]. This is followed by a $\log L^{D-1}/3$ added to the strength J of a spin-spin interaction in the Hamiltonian

$$H = -J \sum_{\langle ll' \rangle}^{\mu_d} \sigma_l^z \sigma_{l'}^z - h \sum_l^{\mu_d} \sigma_l^x, \quad (16)$$

where σ is the spin configuration (spin up +1 or spin down -1) as an assignment of spin value to site l or l' , from the expected sites $\langle ll' \rangle$, where a spin flipping event i or j occurs in the z -direction. For a quantum measurement point [4], this is the expected area of pairwise interactions for producing a GSM, BEC, BEC pairs or entangled EPR pairs, see Eqs. (1), (17), and Example 4.B. The Hamiltonian corresponds to a non-critical spin chain, where its values are plotted in Fig. 4(a), saturating to a constant (area law) [26]. This energy has the periodic boundary conditions $\sigma_{\mu_d+1}^z = \sigma_1^z$, i.e., a finite number of spins on a 1D ring as part of the CNT layer [18–20].

From the BEC EPR pair teleportation model [61,62], for step 2 of Algorithm 2, applying a spin operation to the area $\langle ll' \rangle$ where the beam splitter interacts, a BEC is split into a BEC pair [61,62]. For the BEC pair, as shown in Fig. 3(d), the effective interaction Hamiltonian scaled from Eq. (16), as the potential part is

$$H = (\sigma_l^z + \sigma_{l'}^z)^2 = (\sigma_l^z)^2 + (\sigma_{l'}^z)^2 + 2\sigma_l^z \sigma_{l'}^z, \quad (17)$$

where applying the $\sigma_l^z \sigma_{l'}^z$ operation to two σ^x -polarized BECs, corresponds to an entangling Hamiltonian between two traps, one at l , entangled with the other at l' . This is a correlated system of BEC EPR pairs [61,62], see Example 2.B. A Bell correlations sum of $(2, 2\sqrt{2}]$, [4, Eq. (18)], is predicted from the QDF as $|\langle \mathbf{k}r \rangle| \rightarrow 1$ between the two entangled states $|i_{ll'}, j_{ll'}\rangle$, for which by Eqs. (5)–(10), have the variances $\Delta(\mathbf{k}_{i,j})_{ll'} \rightarrow 0$ and $\Delta(\mathbf{r}_{i_{ll'}} + \mathbf{r}_{j_{ll'}}) \rightarrow 0$, [60, Sec. 6]. This denotes there is a minimum to no variation in the observables of the EPR pair, once entangled across the interval Δt^* , where $|\langle \mathfrak{P} \rangle| \rightarrow 2$ under a QDF transformation, see upper Fig. 1 and Fig. 3(d).

The inverse of the BEC EPR teleportation is superdense coding in Algorithm 2, step 3: the EPR resource is shared as the BEC EPR state over a quantum channel to decode the system's quantum state in classical bits.

System's total energy conditions

There are two total energy conditions of the system. These energy conditions can be derived from any PT via scalar κ field products in Eq. (13), relative to Eq. (15). The expected energy conditions observed from the quantum energy conservation [41,69,73], are as follows.

$$|E\langle f(\kappa)\ell\rangle| = \begin{cases} H\Psi = E\Psi, \text{ as } H = E = \text{const.}, \\ H\Psi \neq E\Psi, \text{ as } E_{\text{in}}^{\Delta t^*}\Psi(t) \mapsto E_{\text{out}}^s\Psi(\tau), \end{cases} \quad (18)$$

where the first condition $H\Psi = E\Psi$ is valid for the total energy $E = H$ being conserved, which is constant in the classical and quantum oscillation models, and time-independent. The second condition $H\Psi \neq E\Psi$ is valid under the Wick rotation $-i\tau = t \mapsto \tau$, corresponding to the thermodynamic events observed from the contour integral [33,34], Fig. 2. The scalar operation in the second condition conserves E quantitatively for H due to a physical fact about systems A and B to contain time. This is based on particle entanglement independent of coordinate choices made on \mathbf{k} and \mathbf{r} between pairwise particles communicating within AB , e.g., Eq. (17). This condition also applies to a non-equilibrium state that can be extrapolated (recording all QDF data via QAI) from a cooling process (BEC) in this system [34,54,72].

A particle's quantum state propagates to system A from one of system B 's lattice sites (of the 4-qubit register), Fig. 1(g). This is through a photon propagator which can assume $e^{-\beta_\tau H}$ between those sites. This propagation occurs between the energy input phase and output phase, as discussed in Example 3.B. The propagator

$$|\Psi(t)\rangle \mapsto |\Psi(\tau)\rangle = \langle \Psi(\tau)|e^{-\beta_\tau H}|\Psi(t)\rangle \quad (19)$$

satisfies $E_{\text{in}}^{\Delta t^*}\Psi(t) = E_{\text{out}}^s\Psi(\tau)$ under the Wick rotation from Eq. (18). However, the condition $H\Psi = E\Psi$ applies to Eq. (16) as a bi-directional QDF, where one direction is, e.g., Eq. (8).

Remark 2. The second condition by its propagator can describe the time evolution of spin operators in Eq. (17). For the deterministic picture, the EPR resource is shared to satisfy superdense coding in the probabilistic picture [4]. This is to predict macroscopic classical states by decoding entangled EPR pairs from the QDF.

Example 4.B. The cat state obeys the following coding model of an ST from [4, Sec. 2.2.1]: $|i\rangle = \{|0\rangle = \begin{bmatrix} 1 \\ 0 \end{bmatrix}, |1\rangle = \begin{bmatrix} 0 \\ 1 \end{bmatrix}, |2\rangle = \begin{bmatrix} 1 \\ 1 \end{bmatrix}\}$ $\otimes (|0\rangle + |1\rangle) \stackrel{\mathcal{T}(i)}{\longleftrightarrow} |i_{ll'}\rangle; i_{ll'} \leq 2$, given that $\mathcal{T}(i)$ is the ST operator satisfying a cat state to undergo a transformation where entangled states are built with orthogonal states of Bob and Alice, e.g., $|01 + 10\rangle$. Entanglement can be expressed as a tensor product

distributes over superposition [8,77], $|i_m\rangle \otimes 2^{-1/2}(|0\rangle + |1\rangle) = |2\rangle$. An ST for $|2\rangle$ as $|0_m\rangle$ occurs within one of the $m > 0$ modes of the ground state $|0\rangle$, where $i_m < 2$. This is a QPT which occurs when a set of atoms are in condensate (degenerate ground states) [4,37]. An ST for $|2\rangle$ appearing in any part of the code is treated as a 3rd state for m sideband levels of $|0\rangle$. Accordingly, in the classical case, $|2\rangle$ turns into $|1\rangle$ when particles diffuse from the GSM. This is a continuous QPT crossover to a CPT [15,16]. For entangled states or those qubit states mimicking Bell states without entanglement, the qubits possess orthogonal and nonorthogonal states, where their product takes the form $|i_m\rangle \otimes |i_n\rangle \otimes |i_{l'}\rangle$ product states [31, pp. 110–112]. This is used in the QDF game and circuit models to represent two bits of information that are hidden, and with an extra qubit in state $|2\rangle$, $|i_m\rangle|i_n\rangle|i_{l'}\rangle \otimes |2\rangle$, reveals the information, as later discussed in Eqs. (25)–(27). Site l , from Eq. (15), can carry a state of an atom that can be flipped or remain in state $|2\rangle$. The inside area of condensate in one of the systems has two sites paired in the s -based (stepwise) area expressed by $ll' = l_s l_s + (2s + 1)$. The area's center has sites $l_0 = 0$ and $l_0 + 1$, and the outer center has two sites $l_1 = l_0 - 1$ and $l_1 + 3 = l_0 + 2$, and so on. The compressed code can appear as the representation of a product state for a set of BEC atoms in the interaction area of pairwise sites

$$E_{\text{out}}^s |i_{l'}\rangle \Psi(\tau) = E_{\text{in}}^{\Delta t^*} \frac{(\mathbf{c}_l^\dagger)^{ll'}}{\sqrt{ll'!}} |2 \dots \underbrace{2}_{l_1 l_1 + 3} \boxed{22} \dots 2\rangle \Psi(t). \quad (20)$$

The diagram shows a rectangular area divided into several regions. At the top, there is a bracket labeled $l_0 l_0 + 1$ above a central site labeled '22'. Below the '22' site, there is a bracket labeled $l_1 l_1 + 3$ below it. The regions are labeled with '2' on the left and right sides, indicating a sequence of sites.

In the code, the possible combination of states is 2^3 for a pairwise site where particles could entangle. This is the product state $|22\rangle$ which can be $\{00, 01, 11, 10\}$ with a probability of $1/4$ pairs being entangled. To decompress the code as a semiclassical approach, the cat state each time is put into a step-by-step loop, leading to a less condensate. This returns a change in entropy $S(\rho_B) = n \log 3 \xrightarrow{\Delta t^*} 0 = S(\rho_A)$, Examples 1–3.B, which satisfies the first condition of Eq. (18) as a reversible thermodynamic process (arrow of time via QAI [44,54,57,74]). The cat state can be expressed in a density matrix $\rho_A = \text{tr} \rho_B$ where condensate occurs inside system B sites. The cat state in a loop of gradual diffusion of the GSM is based on tracing the product state after a CNOT operation

$$\rho_A^s = \left(\dots |02\rangle_{l_0 l_0 + 1} \langle 02|_{l_0 l_0 + 1} + |22\rangle_{l_1 l_1 + 2} \langle 22|_{l_1 l_1 + 2} + |01\rangle_{l_2 l_2 + 3} \langle 01|_{l_2 l_2 + 3} \dots \right) \left[3ll'! 4 \xrightarrow{\Delta t^*} 4ll'! \right]^{-1}. \quad (21)$$

Here, a state is diffused from a pure state $|0\rangle$ relative to Δt^* , as a classical of two or more states. The second element of the trace of the compressed code still needs decoding, as product $|22\rangle \rightarrow |2\rangle$, which can be 0 or 1. The final decoded sequence must be distinct, 0 or 1 from a probe readout using scalar κ applied to the particle field of each site. As in Grover's algorithm [12,13,37], the number of times the diffusion of states from a GSM can be mapped to the Grover iteration and its diffusion operator. In the lens decoding process, the operator operates on the demarcated areas of pairwise qubits in Eq. (21), ranging from $\sqrt{2}$ to \sqrt{N} iterations for a search to obtain a classical state. Here, the GSM is the target for delivering a classical product state to a probe and predict a PT.

Remark 3. Any PT crossover from QPT \leftrightarrow CPT in Example 4.B, is satisfied by $\mathcal{T}(i)$, which can map to the relevant unitary phase shift operators presented in the QDF circuit, e.g., the phase shift measurement of $\omega_{|i_m\rangle}$ for state $|i\rangle$ in Meth. Valid. I. Hereon, $\mathcal{T}(i)$ is self-contained in most equations due to its repeated use in [4], and only limited to phase shift discussions made in the coding part of the QDF.

Remark 4. In Example 4.B, the values of i and j are limited to $j(j \leq i) \in [0, 2]$, where the value 2 denotes any GS or ES of a particle's quantum state $\{|0\rangle, |1\rangle, \dots, |N-1\rangle\} \mapsto |2\rangle$. This determines a QPT or its crossover PT.

Remark 5. In Example 2, the maximum value of κ via α denotes the ST probability applied to a pairwise field over length L doubles the probabilities in the density matrix through a lens function, achieving a pure state.

From Example 2 and Eq. (13) [4, Sec. V. C], the following intervals for Eq. (8) can be derived

$$\Psi(\mathfrak{P}) \geq 2^{-\frac{1}{2}}, \text{ and } |\langle \mathfrak{P} \rangle|^{\frac{1}{2}} \in [1, \sqrt{2}], \quad (22)$$

where zero superposition or separable states are observed once $\mathbf{r}_{j_{l'}}$ is predicted via κ as $|\langle \mathfrak{P} \rangle|^{\frac{1}{2}} \rightarrow 1$, as well as entanglement, if $|\langle \mathfrak{P} \rangle|^{\frac{1}{2}} > 1$, [35] or upper Fig. 1. From Eq. (4) and Fig. 3, for each diverging length L between a pair of particles (strictly measured between a pair of positions in sites l and l'), $\mathbf{r}_{j_{l'}}$ can scale to $|\langle \mathfrak{P} \rangle|^{\frac{1}{L}} L_e \approx 2$.

Event frequency

Consider the following assumptions:

Assumption 1. The probabilities of spin-flipping events by particles in ES and GS, Fig. 2(a), represent the same qubits from the above-mentioned examples.

Assumption 2. From Definition 5, let a trial by a Laplace transform in the system generate a set of output states in three observable quadrants of energy surface $\mathcal{O}_q = \{\mathcal{O}_1, \mathcal{O}_2, \mathcal{O}_4\}$.

Table 1

Energy **input/output** calculations and lens product table. The results are based on the cyclical events or thermal event flow observed between the GS and the ES of the system in Fig. 2. The specific details and analysis of each measurement are presented in [6, Sec. 8], where this table represents the summary of the results for each lens function.

Lens function	Description	Input/output event measurement, or, product magnitude	Interval	Event frequency $ j ^2$
$\mathfrak{L}^+(N)$	Convex lens function	$\left(\frac{E'_{\text{out}} \Phi - E_{\text{in}} \Psi}{E_{\text{out}} \Psi} \right) \xrightarrow{\text{convex}} \left(1 - \frac{\mathcal{O}_q}{\mathcal{O}_q^\parallel} \right)$	$\left[\frac{1}{3}, \frac{1}{2} \right]$	[1, 3]
$ \mathfrak{L}^+(N e^{2i}) $	Convex lens product magnitude	$r_{\mathfrak{L}^+}$	(4, 4.5)	—
$\mathfrak{L}^-(N)$	Concave lens function	$\xrightarrow{\text{concave}} \left(1 - \frac{\mathcal{O}_q^\parallel}{\mathcal{O}_q} \right)$	[0.4, 0.6]	[1.6, 2)
$ \mathfrak{L}^-(N e^{-2i}) $	Concave lens product magnitude	$r_{\mathfrak{L}^-}$	≈ 4	—
$\mathcal{P}_{\mathfrak{L}^+}$	Convex cumulative distribution	$\mathcal{P}(\mathfrak{L}^+(N); \varrho_{B:A} = \frac{3}{4}) = \sum_{i \in \{0,1\}} \frac{\varrho_{B:A}^i}{e^{\varrho_{B:A} i!}}$	[0.47, 0.8]	3
$\mathcal{P}_{\mathfrak{L}^-}$	Concave cumulative distribution	$\mathcal{P}(\mathfrak{L}^-(N); \varrho_{A:B} \geq \frac{1.6}{8}) = \sum_{i \in \{0,1\}} \frac{\varrho_{A:B}^i}{e^{\varrho_{A:B} i!}}$	[0.8, 1)	[1.6, 2)
$\{\mathcal{P}_T; \mathcal{P}_{T'}\}$	Thermal event probability evaluates $\mathcal{P}_{\mathfrak{L}^\pm}$ at $i = 0$	$\{1 - \mathcal{P}_{\mathfrak{L}^+} _{i=0}; 1 - \mathcal{P}_{\mathfrak{L}^-} _{i=0}\}$	{0.53; 0.19}	[1.6, 3]
$\mathcal{Q}_{\mathfrak{L}^+}$	Concave-convex cumulative distribution	$\mathcal{Q}(\mathfrak{L}^+(N); \varrho_{B:A} \geq \frac{3.6}{4}) = \sum_{i \in \{0,1\}} \frac{\varrho_{B:A}^i}{e^{\varrho_{B:A} i!}}$	[0.36, 0.76]	[3.6, 4]
$\mathfrak{L}^- \cap \mathfrak{L}^+$	Thermal event probability evaluates $\mathcal{Q}_{\mathfrak{L}^+}$ at $i \in \{0,1\}$	$1 - (\mathcal{P}_T + \mathcal{P}_{T'})$	0.28	[3.6, 4]
$\Psi\Phi$	QDF function	$(\kappa\Phi \rightarrow 2\kappa^{-2}\ell r) \Phi$	$\left[\frac{1}{e^{2i\kappa r}} \sqrt{\frac{2}{\pi}}, 1 \right]$	$ j ^2 \in \{\mathcal{O}_q \cap \mathcal{O}_q^\parallel\}$
$\Phi\Psi^2$	QDF function for a three particle interaction	$\Phi\Psi^2 \rightarrow \langle \Psi \Psi \rangle \Psi = e^{i\kappa r} \sqrt{L^{-3}}$	$r_{\mathfrak{L}^\pm} \in (0, 1]$	$ j ^2 \in \mathcal{O}_q^\parallel$

Assumption 3. Consider Assumptions 1 and 2. The p 's in form of a sum contribute to \mathcal{P}_T or $\mathcal{P}_{T'}$ measured via the lenses' work done across points of the energy surfaces \mathcal{O}_q and \mathcal{O}_q^\parallel . The probability of a spin-flipping event squared is p_q^2 , and the probability of its complement is $p_q'^2$. These events occur in at least one particle site paired with another in system B , A or between A and B as a quantum event.

Assumption 4. Assume the density matrices from Examples 2–4.B are reused to generate lens products.

From these assumptions, two events can mutually occur in quadrants \mathcal{O}_1 and \mathcal{O}_4 . The magnitude of events (frequency) on the complex and real sides of the contour (energy path) can give two possible output states

$$|j|^2 = |f(o_1, o_4)|^2 = (p_1 + ip'_1)(p_1 - ip'_1) + (p_4 + ip'_4)(p_4 - ip'_4) = p_1^2 + p'_1^2 + p_4^2 + p'_4^2 = 2. \quad (23)$$

Out of the four quadrants, *mutually inclusive* (concurrent) events have the probability $p_1 \frac{1}{4} + p_4 \frac{4}{4} - (p_1 \frac{1}{4} \times p_4 \frac{4}{4}) = 1$. Either event is a thermal event of system A as an ST of an ES or a GS. In \mathcal{O}_2 , another two events give an output state as the input for \mathcal{O}_1^\parallel and \mathcal{O}_2^\parallel , which is

$$|j|^2 = |f(o_2)|^2 = p_{21}^2 + p'_{21}^2 + p_{22}^2 + p'_{22}^2 = 1. \quad (24)$$

These events have the probability $p_{21} \frac{1}{8} + p_{22} \frac{2}{8} - (p_{21} \frac{1}{8} \times p_{22} \frac{2}{8}) = 0.53$ for a GSM, superposed or entangled, that contributes to a thermal event (a PT due to change in temperature) from system B to A . These events can occur in a total of 8 quadrants: 4 parallel subquadrants of \mathcal{O} (quadrants of \mathcal{O}^\parallel) in B , and 4 quadrants of \mathcal{O} in A , Fig. 2(a). Table 1 lists the results of using these probabilities for each lens product relative to its description.

Method validation of lens products

The following sections validate the QF-LCC method by using quantum computers and simulators [5,64–68]. Part I implements the QF-LCA as a QDF circuit on N -qubit machines. Part II compares the results from Table 2 to the measurement outcomes of the QDF circuit in Part I. Part II presents the data analysis summary on the QF-LCA, and validates the QF-LCC method for predicting entanglement with classical measurement outcomes.

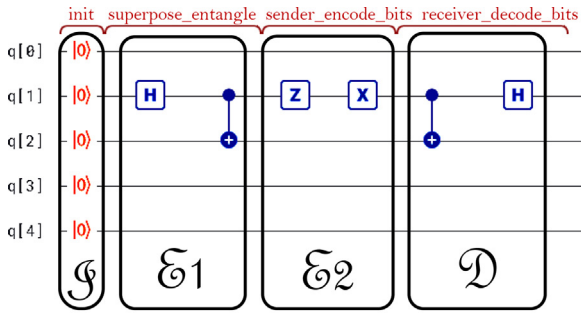
Method testing

Part I presents the method to test the QF-LCA code on: 1- N -qubit machines as QF-LCA circuits, and 2- test QDF operations relative to QF lens distances distinguishing system's classical and quantum states. Part II classifies Part I test results of the decoded qubits

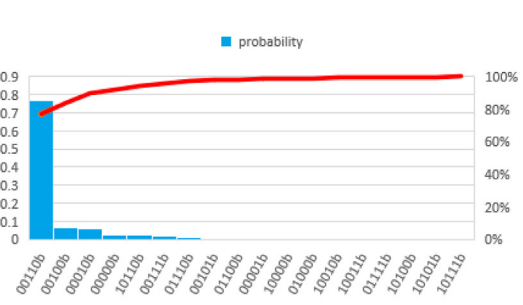
Table 2

Upper table: $|\Delta|$ calculations on [Table 1](#) values. Lower table: S and $|\Delta\mathfrak{L}_{AB}^\pm|$ results are computed between lensing events through the QDF lens relative to Δt^* as a thermal event, as well as entanglement, given the correlation $\langle kr \rangle$ via $|\Delta|$ and d .

$f_{ \Delta }$	$\mathcal{Q}_{\mathfrak{L}^+}$	$\mathcal{P}_{\mathfrak{L}^+}$	$\mathcal{P}_{\mathfrak{L}^-}$
$\mathcal{Q}_{\mathfrak{L}^+}$	0	[0.04, 0.1]	[0.22, 0.44]
$\mathcal{P}_{\mathfrak{L}^+}$	[0.04, 0.1]	0	[0.33, 0.53]
ρ	$\rho_B \xrightarrow{\Delta t^*} \rho_A$	$\rho_A \xrightarrow{\Delta t^*} \rho_B$	ρ_{AB}
S	$[0, n \log 3]$	$(0, n \log 3]$	$\left(0, \frac{n \log 3}{\log 2}\right]$
$ \Delta\mathfrak{L}_{AB}^\pm $	$\left[0.1, \frac{1}{3}\right] L_E^{-D}$	$\left[0.1, \frac{1}{3}\right] L_E^{-D}$	$\left(\frac{1}{2}, 1\right] L_E^{-D}$
	Does not satisfy Eq. (10)	Can satisfy Eq. (10) via Ising model	Satisfies Eqs. (7)–(10) via our model



(a)



(b)

Fig. 4. Quantum circuit design for superdense coding by implementing the core operation of [Algorithm 2](#), steps 1 and 3. (a) The superdense coding sub-circuits initialize the GS qubits from the left, to the point of decoding, right. (b) A Pareto histogram denoting the result of the algorithm executed with 1024 shots on a 5-qubit computer, spin-2 Starmon-5, [65]. The cumulative curve denotes other outcomes with low probability, totaling 1, compared to the simulated fixed outcome of 100% probability on the binary string 00110b. Both histograms from the quantum computer, and a 26-qubit QX single-node simulator [65], respectively, satisfy a high probability $> 2/3$, and a value of 1 as a deterministic (optimized) algorithm (downloadable design and results from [5]).

as registered classical bits from Part I. Part II interprets the classical data and classifies the measurement outcomes for an intelligent (QAI) decision, in order to optimize the thermodynamic system in its performance by predicting its final state with a high success probability.

Method validation - Part I

Quantum field lens coding on N -qubit machines

Quantum computers [12,13,64] can be used to implement and evaluate an equivalent quantum circuit for the QF-LCA. For example, one can evaluate the non-deterministic and deterministic behaviour of the algorithm by measuring the entanglement length between particles relative to their continuous random states projected in a quantum experiment. The QF-LCA can be simulated by incorporating QFT components [44,51,66,76] under a κ -based QDF transformation and compression [45–47,64–66] in the circuit.

Circuit background and implementation of QF-LCA

The superdense coding part of the following code after execution on a 5-qubit processor, Starmon-5 [65], demonstrates a probability $> 2/3$, [Fig. 4](#). A probability close to 100% from IBM [64] and QI [65] simulators has also been observed. Superdense coding is the core of the EE scaling implementation of [Algorithm 2](#), and shapes the lens coding externals as the compression and decompression steps from [Example 3.B](#) and [Algorithm 2](#).

The analogy between the expected probabilities from the following quantum circuits (algorithmic) events and those of a QDF game can be found below. This game is performed between Alice the host ♠, Bob the guest ○, Eve ♣ and/or the audience ♦ of a quantum game where a prize ★ is to be won by Bob if he chooses the correct box ■ with the prize, like a quantum particle in a box [4,11,15,41]. Any prize state $|i_m\rangle$, poor or else mapping to “the prize” as Bob’s TS or Alice’s TS [4, Sec. 1] can be defined by $|i_m\rangle_{\star \in \{\blacksquare, \square\}}$ in the game space, [Fig. 8](#). Alice’s TS is to expect Bob does not attain his TS as ★, and maintain state □ for the box against him. As shown in [Fig. 8](#), the prize for any prize state between sites l and l' (or two boxes) as an entangled EPR state, can be defined by $|i_{ll'}\rangle_{\star \in \{\blacksquare, \square\}}$ in the same space, as discussed in [Example 2.B](#).

The role of each game participant in the QF-LCA, according to [4, Sec. 2.2], is defined as follows.

Table 3

Specifications table of game participants predicting states corresponding to game events in QDF space [4]. All outcomes are based on calculating κ and the field transformation between the system energy input and output. The κ -based field transformation occurs between Bob's field and other participants as listed under “photon.” The photon projects state j onto Bob's field at his decision point (left two columns), and that state depending on i_m and i_n values, determines the outcome (from middle to right columns). An *uncertain* outcome is when the quantum information on the κ -based field transformation is not accessed by Bob.

$ i_m\rangle$ via $j \in ij\rangle \rightarrow i_m i_n\rangle$	State projected by photon	ΔE in GS/ES; $ \Delta i $; i	Box prize state $ i_m\rangle$; particle example	κ -based outcome
$ 1\rangle$ via $ 12\rangle$	Eve via Alice	$2E_0$ in ES; 1; 1	box with prize; remaining box is 0 prize	certain
$ 0\rangle$ via $ 01\rangle$	Alice to Bob	$2E_0$ in ES; 1; 0	prize is suggested to Bob; Bob predicts 0	certain
$ 1\rangle$ via $ 11\rangle$	Eve via Alice	$0; 0; i_m = i_n = 1$	prize is entangled with Bob or Alice	certain
$ 0\rangle$ via $ 00\rangle$	Eve via Alice	$0; 0; i_m = i_n = 0$	0 prize is entangled with Bob or Alice	certain
$ 0\rangle$ via $ 02\rangle$	Alice or Audience	$4E_0$ in GS/ES; 2; —	prize is in superposition: poor or else	uncertain
$ 1\rangle$ via $ 10\rangle$	Alice or Audience	$2E_0$ from GS; 1; —	prize is hidden while Bob decides	uncertain

1. Alice is a photoprobe who e.g., observes a photon from a scattering event at a pairwise particle interaction site [6,50]. Alice measures the energy state at a pairwise point, which is the *quantum readout point* [4] from the expected area of pairwise interactions $\langle II' \rangle$ in a particle scattering event (the sum of interactions).
2. Alice can also project her energy state onto Bob's space as the source of light or information, or a photon.
3. Bob is an atom where other particles such as Alice interact with.
4. An audience member is a photon projecting onto Bob's state, for or against Alice's projected states.
5. Eve is a photon, a photoprobe or an atom interacting with any of the above-mentioned particles.
6. The prize is a quantum particle that can reduce its energy to a lower energy state via absorption as a prize.

As shown in Table 3, to represent the prize energy state, the minimum number of qubits to be used is 2 denoting prize superposition. The number of operations required to perform and measure on a 5-qubit machine is satisfied by the total number of particles initiated: 5 qubits as Alice, Bob, Eve, an audience member, plus the prize. The prize is hidden by Alice in one of the three boxes. The prize is in state 1 which makes Bob, if he correctly predicts it, the winner. The prize is in state 0, which denotes an empty box with no prize, if Bob assumes and predicts the wrong box to be with the prize. Anything in between states 0 and 1 (sidebands), is a *prize* as a poor imitation of the *prize* with a pure energy state of 1 [4, Sec. 1]. Here, the assumption is that some energy of the system is contained in a different trap by e.g., Alice who set up a BEC EPR pair from a BEC particle in Example 2.B. The remaining system's energy due to environmental effects and other particles interacting with the BEC particle, altogether are in a mixed system state, and not revealed to Bob. This state can be decoded from a qubit site-to-site (box-to-box) teleportation and superdense coding in the QDF circuit.

The measurement outcome of each state is shown in Table 4 by implementing the QDF circuit for distinguishing Bell states, by eliminating $n - 2$ possible states from the Bell measurement, and determine the two hidden bits of information. This is achieved by introducing Eve's nonorthogonal states [31] denoted by an extra qubit to be in any nonorthogonal state of $|2\rangle$ as the third state to a particle pair. This yields definite information with certainty out of the two remaining possible states. Eve is the third particle paired with Alice or Bob, as the vital party needed to reveal the hidden information about the prize position from $|\langle \mathfrak{P} \rangle|$ to Bob, or any other participant of the game. This is possible through the measurement process of qubit state elimination from the following equation, which is by using the extra qubit required to reveal the hidden information [4,31].

For all particle pairs in the QDF circuit, the qubits via $f(\kappa)$ transform into a sum of superpositions. From Eqs. (2), (3) and (12), this is the sum of tensor products \pm operations for maximally entangled states

$$\sum_{1 \leq l \leq \mu_{ij}}^{3 \leq \mu_{ij} < \infty} \left| \frac{\langle 2\mathbf{r}_{i,j} | f(\kappa) \ell \psi_{ij} \rangle}{|\langle \mathfrak{P} \rangle|^{1/2}} (|0_m i_n\rangle \pm |1_m i'_n\rangle) \right|_l, \quad (25)$$

where i'_n is the negation of i_n as the target qubit. For any l , field position(s), there is a temporal QDF correlation function $|\Theta(2\ell r)|_l$, which evaluates $\mathbf{r}_{i,j}$ as $\mathbf{k}_{i,j}|\mathbf{r}| \rightarrow |\mathbf{kr}| \rightarrow 1$ via κ from Eq. (6) and [4, Sec. 5].

Any value of $\lambda_c > 1$ that satisfies $d \rightarrow 1$, denotes an energy increase revealing the prize position in $|\langle \mathfrak{P} \rangle|^{1/2}$ from the sum of $|\Theta(2\ell r)|_l$ in Eq. (25), [4,63, Sec. 5.3]. For Alice, Bob, Eve and the audience, the locally indistinguishable Bell states component of the equation can be written as a set of distinguishable Bell states

$$\Theta(2\ell r) |ij\rangle \otimes |i_{ll'}2\rangle = \Theta(2\ell r) (|0_m i_n\rangle \pm |1_m i'_n\rangle) \xrightarrow{\text{distinguishable}} \otimes |i_{ll'}2\rangle_{\mathbb{V}}, \quad (26)$$

where any of the vital set elements $\mathbb{V} = \{\spadesuit, \clubsuit, \diamondsuit, \blacksquare, \star\}$ in the game globally holds nothing of value, as its possible states are all nonorthogonal, denoted by $|2\rangle$ in $|i_{ll'}2\rangle$. However, locally, the element is vital to reveal the hidden information to Alice, Bob or Eve as $|i_{ll'}\rangle$ in $|i_{ll'}2\rangle$. As in [12], the Schrödinger's cat is in a superposition state like the prize in a box, and not necessarily entangled. The light source by Alice, as observed by Eve, projecting randomly polarized light onto the particle in the box, is in a mixed state. However, the cat as the BEC atom, the photon, the photon detector or photoprobe, and their environment *together*, are in a pure state as we construct a product of their states below [4, Sec. 2.2]. Hence, an extra qubit is required to render distinguishable states.

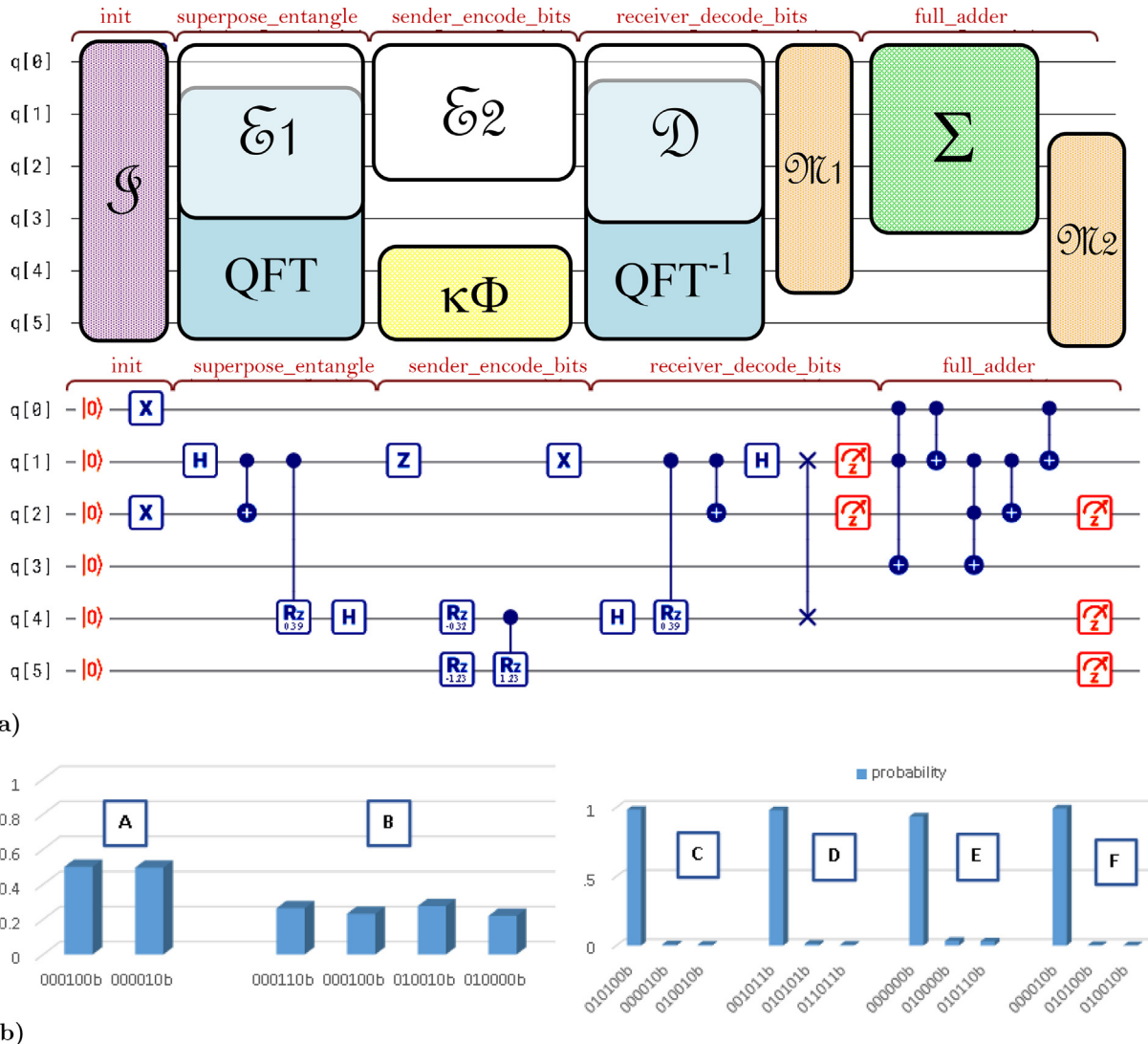


Fig. 5. (a) Quantum circuit design for superdense coding by implementing Algorithm 2 core and exteriors: counting the spin flips, and QFT under a κ -based QDF transformation. (b) Circuit measurement outcomes (b)A–(b)F as highlighted. These outcomes are determined based on reconfiguring the circuit design in different trials, such as changing the direction of the scalar field between circuit measurement points. One of which is conforming non-entangled states (classical bits) to an entanglement point for an EE measure (to determine a PT), as presented in Fig. 6. The corresponding circuit design code and results can be downloaded from [5].

For distinguishing states *without entanglement*, the product states mimic the Bell state structure as quasi-Bell states, i.e., any local measurement made by any participant will render one of the possible pairs of states indistinguishable. The distinguishable against indistinguishable measurement outcome can be expressed by

$$\Theta(2\ell r)|ij\rangle \otimes |i_{ll'}2\rangle = \Theta(2\ell r) \underbrace{|i_m\rangle_{\{\blacksquare, \clubsuit\}}|i_n\rangle_{\{\circlearrowleft, \clubsuit\}}}_{\text{indistinguishable}} |i_{ll'}\rangle \vee |2\rangle_{\{\clubsuit, \clubsuit\}}, \quad (27)$$

where Eve \clubsuit , can reveal the information on the prize's expected site $|ll'\rangle$ possessing the prize state which can pair up with Bob or the audience, revealing the hidden information about the prize position to any other participant, as shown in Fig. 8. This particle pairing action does not require entanglement since there is an extra qubit shared by a third party in the probabilistic picture [4, Sec. 2.2]. In the QDF circuit, a SWAP and no SWAP gate represents this operation given the prior probability values of pairwise states measured, Fig. 7, which is a classical “IF statement” switch. For example, if the prize is spotted by one of the vital parties, thus reveals the hidden information using its qubit. This is shown in the superdense coding portion of Code Listing 2, with binary results in lower Table 5. In Fig. 8, the symbol \clubsuit can switch to \spadesuit as a chosen quantum measurement point at $2\ell r$ in Eq. (1), for Eve to perform Bell measurements within a QDF. Eve in the deterministic and probabilistic pictures, like Alice, is vital to reveal the hidden information

to other parties during Alice's system state change (to one of the prize states) and prior to Alice's final measurement (game outcome). Eve possesses nonorthogonal states [31], who can in the QDF communicate the message via superposition and entanglement of other parties as EPR pairs in the deterministic picture, Eq. (26). Eve, as in superdense coding, from the QDF circuit shares the extra qubit to reveal the hidden information in the probabilistic picture, Eq. (27) and Remark 6.

From the following code, Alice via superposition sends 1/2 part of the message about the prize position to herself as the receiver in a different location to challenge Bob. The other half of the message is also known to Alice as she can superpose between boxes to see where the prize is hidden from Bob and the audience. The part of the message about one of the boxes with no prize is transmitted to Bob, where Alice asks Bob where the prize is between the two remaining boxes. Bob chooses a box, and Alice, or the audience asks Bob to pick a Box as they suggest, or let him stick to his initial choice. If Eve via her superposition and entanglement abilities, intercepts and gathers information from Alice (her 1/2 part of the message unknown to Bob about the prize) and shares it with Bob, the probability to win is 100%. On a 5-qubit machine, the probability can fall within the interval $(2/3, 1]$, due to prize superposition. If Bob entangles with the superposing prize in any box via the CCNOT operation (a full-adder, or by keeping a record on its moves between boxes), he will win all the time, see machine learning classifiers discussed on Eq. (37).

In Figs. 4 and 5, the transparent and color-coded layers as functions \mathfrak{I} , \mathcal{E}_1 , \mathcal{E}_2 , \mathfrak{D} , respectively, denote qubit initialization, first encoding, second encoding, and decoding sub-circuits. A sub-circuits is labelled by name e.g., $.init$ from Code Listing 1 is $init$ for \mathfrak{I} in both figures. In the upper Fig. 5(a), the transformation operators are QFT, $\kappa\Phi$, QFT^{-1} , whereas \mathfrak{M}_1 , Σ , and \mathfrak{M}_2 , respectively, denote the 1st measurement, the adder, and the 2nd measurement of the circuit. The QFT via the κ -based QDF transform as a momentum operator reads QFT^{-1} for decoding, prior to measurement. The kinetic and potential (for trapped particles) operations written in their coordinate representations are given by Eq. (30), or [51]. This, for example, satisfies the transformation $\kappa\Phi \rightarrow \Psi$ as $\Psi(\Psi)\langle\Psi\rangle$ from Eq. (8), which supplies information about the prize position to the observer at \mathfrak{M}_2 . This information is obtained by registering maximum entanglement via phase gate $\pi/2$, implemented after line # 50.

The expected outcome of a game event corresponds to any particle collecting information about the prize state entangled with its opposite state in a box, or an assumed prize state as an attainable TS by any participant, such as Bob [4, Sec. 1]. This is equivalent to the maximally entangled state at $\pi/2$, where R_{zz} gate is equal to a two-qubit interaction $R(Z \otimes Z)$, and is symmetric [64]. This is obtained via the κ -based QDF transform, i.e., a $\pi/2$ entanglement outcome via a $\pi/8$ qubit shift, which is equivalent to a qubit $\pi/8$ T -gate (one used to produce an EPR pair) [61,64]. This gate operates within the QFT circuit model by [49,64], using SWAP gates and multilevel control gates (operations), in a D -dimensional qudit space [49]. The two-qubit gate transforms the input state into an entangled state, i.e., the superposition of pairwise frequency modes (phase) as follows.

Implementation of QDF operators

The quantum circuit can have an extra layer as an interaction potential barrier implemented [51]. The barrier denotes BECs in system B 's multi-well CNTs, Fig. 1. The quantum lens distance between Figs. 1(a, d, g), scales to entanglement length L_ε , observed between a particle pair in systems A and B . The concepts of quantum tunneling [36,43] and PNS attack [4, Remark 1], can be used to determine the loss or unaccounted energy (hidden information) of the prize when entangled as an EPR pair from Eq. (17), during quantum communication, Examples 2.B–4.B. This is satisfied by measuring EE which is lens distance-based between pairwise lensing events which scales to L_ε , Fig. 3. The lens distance between particle pairs per event as a dimensionless quantity is

$$\Delta L_d = \overbrace{|l - L_d|}^{\Delta L_d} \overbrace{L_d/2^n}^{\Delta l}, \quad \text{and} \quad L_d = \lceil Ld^{-1} \rceil, \quad (28)$$

where Δl satisfies the wavefunction discretizing L into 2^n -points stored in an n -qubit quantum register, and L_d rounds the value of length L between two particle sites (qubits), which can scale up to L_ε , relative to lens distance d from Eq. (9). In this design, $q[l]$ is the controlled qubit, and $q[L_d]$ is the target qubit. For example, the logarithmic scaling of EE in the system, Fig. 3, can be expressed via an *interaction operator* [51]. The interaction operation is applied to qubits $q[1]$ and $q[2]$ in Fig. 6 (or $q[1]$ and $q[4]$ in Fig. 5), which, respectively, act on two particles, one in system A , and the other in B , Fig. 1. The selection of a qubit pair in this operation must meet the qubit configuration (matrix) in the circuit prior to any count made by the adder. In Fig. 6, qubits $q[2]$ and $q[3]$ (like in Fig. 5), are respectively measured as *CarryIn_SumOut* and *CarryOut* at the phase shift measurement [64,65]. This measurement is $\mathfrak{M}_2(\omega_{|l\rangle}, \Delta t^*)$ from Eq. (30), where the readout of state $|l\rangle$ is obtained after the operation on the pair $q[1]$ and $q[2]$. For this operation, a diagonal matrix relevant to [51] is constructed after taking the phase $e^{i(2/\lceil L \rceil \Delta l)c\Delta t \rightarrow i(2/\Delta l \Delta L_d)}$ as a common matrix element. A phase value of 1 is obtained as $\Delta t \rightarrow 0$, given $\Delta l \leq \infty$ by a photoprobe lens projection onto (or scattering off of) particle-pair space under a QDF transformation. This is obtained from the *interaction potential energy operator* $\omega_{|0_m\rangle} = e^{-\beta_r E_{i_m}}$, via Eqs. (11), (12), (15), and Example 4.B, as

$$\begin{aligned} \mathcal{E}\mathcal{E}_2(\omega_{|0_m\rangle}, \Delta t^*) &= e^{\text{diag} \left(\underbrace{\overbrace{t/\Delta l}^{\text{reflection of the left matrix elements}}}_{\rightarrow 0}, \frac{1}{\Delta l}, \frac{3t/2\Delta l, 5t/3\Delta l, 5t/3\Delta l, 3t/2\Delta l, t/\Delta l, 0}{\Delta l} \right)} \\ &= \text{diag} \left(1, e^{i/\Delta l}, e^{3t/2\Delta l}, e^{5t/3\Delta l}, \underbrace{e^{5t/3\Delta l}, e^{3t/2\Delta l}, e^{i/\Delta l}, 1}_{\text{reflection of the left matrix elements}} \right), \end{aligned} \quad (29)$$

```

1 #-----#
2 # A quantum field lens coding algorithm by a conventional quantum circuit
3 # written in cQSAM, Ref. [48].
4 #
5 qubits 6 # Initialize a 6-qubit register (define the number of qubits)
6 .init
7 prep_z q[0:5] # State initialization on 6 qubits in the z-basis in the |0>
8 # state; Initialize inputs to some values
9 #
10 #-----#
11 # q[0] --> |A>
12 # q[1] --> |B>
13 # q[2] --> CarryIn_SumOut
14 # q[3] --> CarryOut
15 #
16 #-----#
17 # Initialize inputs A=1, B=0 and Carryin =1 to perform addition after
18 # decoding Alice's message about the prize position
19 {X q[0] | X q[2]}
20 #
21 #-----#
22 # Define the combined superposition and entanglement sub-circuit as
23 # .superpose_entangle for superdense coding
24 .superpose_entangle(2) # Iterate up to i=2 times (third party encodes qubits);
25 # any i>2 times for any other scenario
26
27 H q[1] # Create a superposition of two states
28
29 cnot q[1], q[2] # Entangle two qubits via CNOT gate
30
31 CR q[1], q[4], 0.39 # Controlled phase shift (or T-gate equivalent, Ref. [47])
32 # gate between qubits 1 and 4 with an angle of 0.39 radians = pi/8 degrees
33 H q[4]
34
35 .sender_encode_bits(1) # From superdense coding scheme, Alice sends two
36 # classical bits as one qubit to receiver
37 Z q[1]
38 {Rz q[4], -0.32 | Rz q[5], -1.23}
39 # (Rz q[5]) is the controlled rotation on ancilla qubit 0, mapping to ((pi^2)/8
40 # + (pi/2)/30) rad or <= pi/2 degrees; The system is evolved to its excited states
41 # when the measurement on the ancilla qubit is in state |0>. Meanwhile, the system
42 # is purified to a state that is close to its ground state (steps of decompression
43 # discussed in the EE measurement section) as measurement takes place to observe
44 # its excited state |1>, Refs. [42, 43, 44, 45, 46].
45
46 CR q[4], q[5], 0.39
47 X q[1]
48 # .middle_recorder(1) or Eve gathers information from Alice with increased certainty
49 # and sends info to Bob (see the QDF game model presented in Refs. [13, 41])
50
51 .receiver_decode_bits(1) # Bob as receiver
52 # decodes bits within two consecutive steps of the game; below Eve collects information
53 # from Alice relative to Bob as .middle_recorder(1) which defines a single step of
54 # kappa-based QDF transformation = a momentum (kinetic energy) operator (Ref. [51])
55 H q[4]
56 CR q[1], q[4], 0.39
57 cnot q[1], q[2]
58 H q[1]
59 SWAP q[1], q[4] # SWAP gate on qubits 0 and 1 after the quantum field (QDF) transformation
60
61 measure_z q[1:2]
62
63 # Perform addition
64 .full_adder(1)
65 toffoli q[0], q[1], q[3]
66 cnot q[0], q[1]
67 toffoli q[1], q[2], q[3]
68 cnot q[1], q[2]
69 cnot q[0], q[1]
70
71 measure_z q[2, 4, 5]
72 # Measure the sum output from qubit 2 and the controlled rotation as momentum (kinetic
73 # energy) operator Ref. [51].

```

Listing 1. Quantum circuit code for Fig. 5(a) written in QI [65] ran on a 26-qubit QX single-node simulator [58]. By removing the relevant circuit components from this code, the superdense coding circuit for Fig. 4(a) can be reproduced to run on a 5-qubit processor, which is implemented between lines # 5–7, 28–30, 37–49, 58–60. This code can be downloaded from [5]. This reference is Listing 1 [48].

where $\mathcal{E}\mathcal{E}_2$ is the entanglement encoding function after superdense encoding \mathcal{E}_1 from the quantum circuit. The *interaction potential* and *interaction kinetic energy operators* can be deduced from the quantum state propagation in real time under the Wick rotation $t = \tau t$, Eqs. (15)–(19), and macroscopic superposition of state $|i_m\rangle$ (a cat state) between l and l' sites, Eqs. (12), and (15)–(20). The conditions to evaluate these operators are as follows.

$$\omega_{|i_m\rangle} = \begin{cases} \omega_{|0_m\rangle} = \omega_{|2\rangle}, & \text{if } \overbrace{|0_m\rangle \leftrightarrow |i_{ll'}\rangle}^{\text{QPT}} \Psi(\tau) = |2\rangle \Psi(t) \\ \omega_{|1_m\rangle} = \omega_{|1\rangle}, & \text{if } \underbrace{i_m = i_n}_{\text{CPT}} = 1, \text{ or } \underbrace{|1\rangle \Psi(t)}_{\text{QPT} \rightarrow \text{CPT}} \end{cases}$$

and the expected measurement outcome is from a phase shift measurement

$$\mathfrak{M}(\omega_{|l\rangle}, \Delta t^*) = \begin{cases} \mathfrak{M}(\omega_{|2\rangle}, \Delta t^*) = |2\rangle \mapsto \Delta E(M \geq 0), \\ \mathfrak{M}(\omega_{|1\rangle}, \Delta t^*) = |1\rangle \mapsto \Delta E(M = 0), \end{cases} \quad (30)$$

where the measurement of $\omega_{|0\rangle}$ denotes the potential energy state $\Delta E(M > 0)$. The crossover to a kinetic state of energy $\Delta E(M = 0)$, or CPT, is via superposition, see [Example 4.B](#). The kinetic component $\omega_{|1\rangle}$ denotes the likelihood of a CPT outcome, which satisfies a QDF transformation after a small time interval Δt^* , [Eq. \(35\)](#). The phase $\omega_{|i_m\rangle}$ for state $|i_m\rangle$ via $j \in |ij\rangle \rightarrow |i_m i_n\rangle$, [Table 3](#), maps to the pairwise particle interaction phase $\omega_{ll'} = e^{-2m\mathbf{k}\mathbf{r}} e^{-\Delta N \mathbf{k}\mathbf{r}}$ from [Eq. \(31\)](#) as a QDF lens function $\Psi\Phi$ from [Table 1](#). The interaction phase is due to a lens projection by $2n$ photons from their probe's field, as discussed below, which satisfies entanglement between particle pairs. This is shown in [Fig. 3](#), relative to the wave propagation factor $e^{-2\mathbf{k}\mathbf{r}}$ described by [Eq. \(31\)](#).

The probability measure of a convex lens product in a QPT is based on ι factored into the transformation from [Eqs. \(6\)–\(8\)](#) as $\kappa\Phi \rightarrow 2\kappa^{-2}\ell r = \Psi\ell d(\mathbf{r}_{i_{ll'}}, \mathbf{r}_{j_{ll'}})$ in [Fig. 2](#). From [Eqs. \(7\)–\(22\)](#), the lens product is

$$\Psi\Phi = (\kappa\Phi \rightarrow 2\kappa^{-2}\ell r)|\Phi = \lim_{|\mathbf{k}\mathbf{r}| \rightarrow 1} \sqrt{\frac{k}{2\pi}} \int_{\text{all } \mathbf{r}} \frac{\psi(\mathbf{r}, t)}{e^{2\mathbf{k}\mathbf{r}}} d\mathbf{r} = \frac{1}{e^{2\mathbf{k}\mathbf{r}}} \sqrt{\frac{2}{\pi}}, \quad (31)$$

where the integral bounds are between 0 and r within the quadrants of \mathcal{O}^\parallel for all \mathbf{r} of this product, [Fig. 2](#). This is assuming Φ is normalized, so that its integral from $-\infty$ to ∞ equals 1. The average momentum $\langle \mathbf{k} \rangle$ is computed from $\psi(\mathbf{r}, t)$, as the QDF projects the product onto the complex plane at $r_{\mathbf{k}\mathbf{r}} \approx 1$. This applies to general cases of QPTs occurring in the CNT layer, as the QDF projects from $B \leftrightarrow A$ space, producing mutually inclusive lensing events in $\mathcal{O}_q \cap \mathcal{O}_q^\parallel$, see [Table 1](#). There are $2n \leq N$ photopropes projecting onto the particle-pair space via the convex lens integration around left and right contours in [Fig. 2](#). The propagation factor in [Eq. \(31\)](#) alters to a pairwise particle interaction phase $e^{-2m\mathbf{k}\mathbf{r}} e^{-\Delta N \mathbf{k}\mathbf{r}}$ within the QDF, [Eqs. \(3\)–\(9\)](#) and [\(33\)](#).

As n from $2n$ -EPR pairs in [Eq. \(32\)](#), tends to $N/2$, the degrees of the phase would map to the scattering factor $e^{i\mathbf{k}_{ij}\mathbf{r}} \rightarrow e^{i\mathbf{k}\mathbf{r}}$ from [Eq. \(6\)](#), where EE is measured, [Figs. 1\(g\)](#) and [3](#). For a single qubit observed using a Bloch sphere [55], and from [Eqs. \(4\)](#) and [\(28\)](#), its distance changing phase relative to a target qubit, has the expectation value $\langle L_d \rangle \in [1, N]$. This is the expected length relative to d , where its values map to the range of a singlet state of $2n$ qubits. The range is given by the inequality

$$\lim_{n \rightarrow N/2} |\langle \mu_d \rangle| = \left| \frac{\langle \Delta N \rangle}{\sqrt{\langle L_d \rangle}} \right| \leq \left| \frac{1}{\sqrt{[1, N]}} \left[\frac{N^2 - N}{2N} \right] \right| = \sqrt{\ln 2} \left| \left[\frac{\ln 2^{n/2-1}}{\ln 4} \right] \frac{1}{\sqrt{\ln 2^{n/2}}} \right| \in \left[\frac{\sqrt{N}}{\sqrt{2}}, \infty \right), \quad (32)$$

where according to [Eqs. \(3\)](#) and [\(4\)](#), $N/2 = \log_2 2^n$, and $\Delta N \leq \mu_{ij}$ from

$$\Delta N = (\mu_{ij} - 2n) \leq \mu_{ij} \quad (33)$$

interactions. To store data about a QDF transformation, $N = 2^n$ in all cases, which maps to a number of storables data points L_d for the circuit, as discussed above (compare this to QFT for a large N by IBM [64]). The result is evaluated based on natural log (converted from log base 2 for a classical bit), to determine the uncertainty in the kinetic and potential energy between particles, [Code Listing 2](#). The results of the magnitude of $2n$ sampled and non-sampled particles, $-N$, are shown in [Fig. 7](#) and [Table 3](#).

In [Table 3](#), to measure the expected energy, two cases of ΔN from [Eq. \(32\)](#) are compared and analyzed:

$$\langle \Delta N \rangle = \begin{cases} \text{Case 1: } \langle \Delta N \rangle = \mu_{ij} \text{ for } |\langle \mu_d \rangle| = \left| \left[(N^2 - N)/2N \right] / \sqrt{N} \right|, \\ \text{Case 2: } \langle \Delta N \rangle < \mu_{ij} \text{ for } |\langle \mu_d \rangle| = \left| \left[N^2/2N \right] / \sqrt{[1, N]} \right|. \end{cases} \quad (34)$$

The two cases are compared relative to the quantum mechanical expectation values as Case 1 results in [Table 4](#). The Case 2 column shows an interval where its upper bound denotes integers of the diagonal elements in [Eq. \(29\)](#), as listed in the highlighted rows. These values are based on the distance measured between two particles with their state described by ψ_{ij} relative to an ST probability from [Eqs. \(10\)](#) and [\(13\)](#). The highly probable outcome of an ST for a particle pair, is expressed by the binary-to-decimal function of a qubit state $b(|ij\rangle)$. This is shown in the $\langle \mathfrak{M}(\mathcal{P}, \psi_{ij}) \rangle$ -column of the table. The expected sum of the conversion between states $|0\rangle$ and $|2\rangle$ with a $P_{|ij\rangle} \geq 2/3$ via the encoding-decoding process, is shown in the rightmost column of the table.

For example, take a pair of particles interacting during the interaction phase $\omega_{ll'}^{-2\pi ij} = e^{-2m\mathbf{k}\mathbf{r}} e^{-\Delta N \mathbf{k}\mathbf{r}}$ between their fields, [Eq. \(33\)](#). From the two cases of $\langle \Delta N \rangle$ intervals shown in [Table 4](#), the value $1/\sqrt{2}$ for one of the sampled particles is a factor of $1/2\sqrt{N}$ from the total particle population. This is the quantum mechanical expectation value of the tensor product $|i_m i_n\rangle \rightarrow |ij\rangle$ as $|i_{ll'} j_{ll'}\rangle$ from [Eq. \(22\)](#) in a Bell singlet state [37,78], given $\mathbf{r}_{i,j}$ and $\mathbf{k}_{i,j}$ value, see [Remark 4](#) and [Definition 3](#). The expectation value can be used to encode a qubit into an entangled qubit state of different qubits as product states to correct a possible qubit flip error in the circuit. For example, any product states can be encoded into an entangled state of triplet qubits [37], or $3[n, 2n \leq N]$ physical qubits in [Fig. 1\(g\)](#), in case of singlet and EPR pairs, to correct that qubit flip error [4, [Remark 5](#)].

The conversion of the qubit states to classical bits after each encoding operation is decoded at \mathfrak{D} , with a high probability outcome measured against its complement. The results correspond to the values listed in the columns following the two cases. By applying the SWAP gate operation from [Fig. 6](#), the expected measurement outcome, based on [Eq. \(30\)](#), is shown in the rightmost table cells. The expected measurement outcome corresponding to $n = 4$ and 5, is for a qubit state $|i_m\rangle$ paired and mixed with state $|i_n\rangle$, as observed in a GS prior to pairwising. The outcome corresponding to N ([Table 4](#), bottom row), is also consistent with the highlighted cell results prior to these two cases of n . This includes determining any expected phase shift from the spin Hamiltonian, $\langle \Delta H^+ \rangle$, under a QDF transformation at a given time step. The summary of the expected measurement results and prediction in [Table 4](#), is illustrated in [Fig. 7](#).

From [Eq. \(32\)](#), the comparable factor $1/\sqrt{N}$ in the inequality expresses a QDF transformation via QFT [64] on an EE scale for $L \rightarrow [0, 1]L_E$. This measurement determines how many particles have been entangled and fall within one or more of the intervals

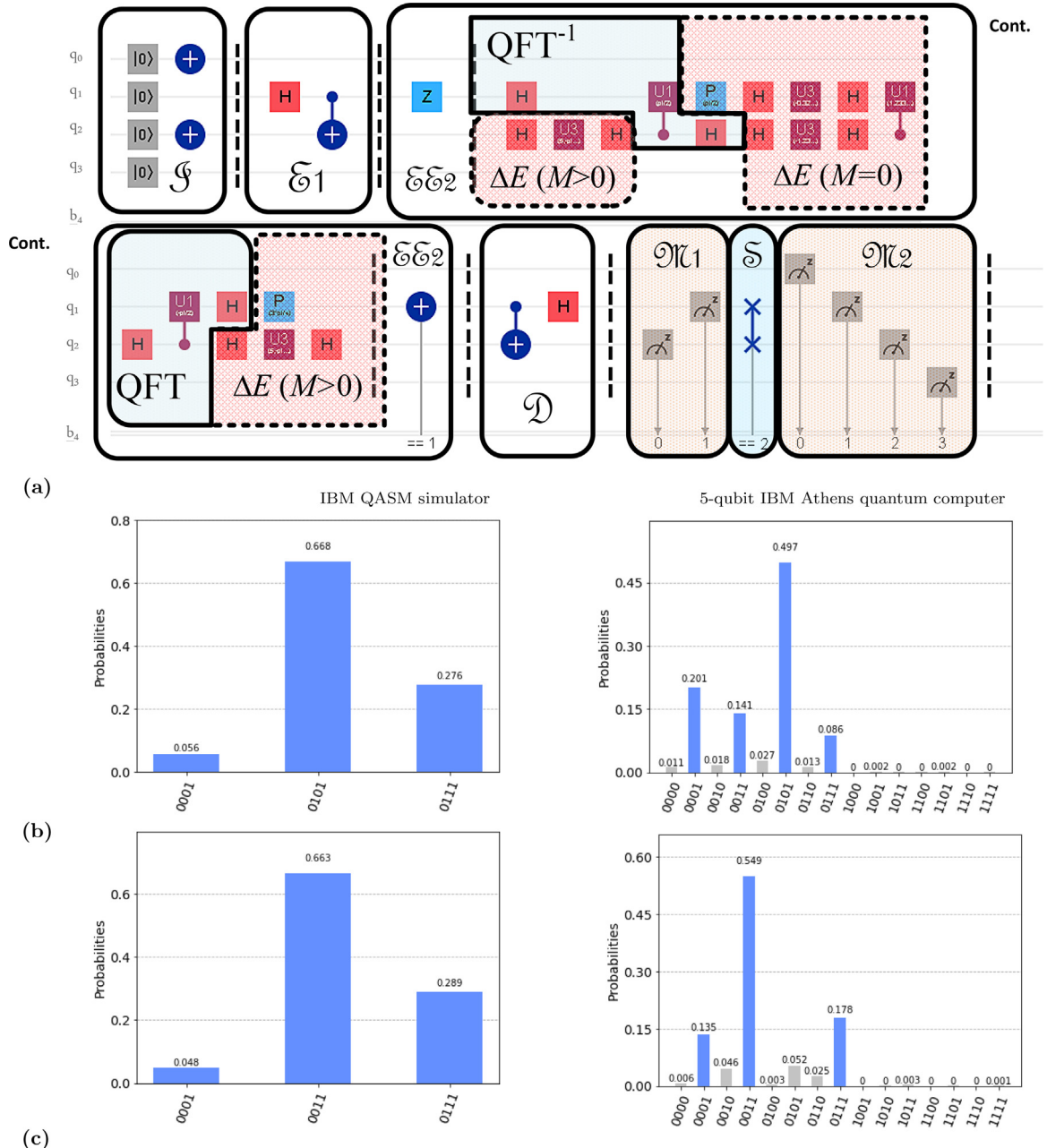


Fig. 6. (a) Quantum circuit design for superdense coding by implementing the core operation of Algorithm 2 and all of its exteriors from steps 1–3. From the QDF transform, non-entangled states can be conformed to an entanglement point as one of the quantum game events for Bob to win. Entanglement entropy can be measured via $\Delta/\Delta L_d$ in Eq. (28), where length L between two particle sites, e.g., Bob and the prize, can scale to $L_{\mathcal{E}}$ within the entanglement encoding layer $\mathcal{E}\mathcal{E}_2$, Eqs. (29)–(35). In this layer, data points are stored by the quantum and classical registers, q_0 – q_4 and b_4 . In the quantum circuit, the sequence of qubits is decoded in classical binary b_4 , where from between qubit registers q_1 and q_2 , Bob can win a prize, the prize, or lose as a possible outcome based on probabilities P 's $\geq 2/3$ vs. P 's $\geq 1/3$. (b) and (c) Circuit measurement results obtained from ‘IBM QASIM simulator’ (left graphs) and a 5-qubit ‘IBM Q Athens’ quantum computer (right graphs). Both, the theoretical and experimental results have been obtained after 8192 shots (iterations). The probabilities of these outcomes are determined based on a QDF transformation, relative to non-entangled states conformed to the point of entanglement for an EE measure (or download code and dataset from [5]).

calculated for $|\Delta\mathfrak{L}_{AB}^{\pm}|$ and S in Table 2. The expected interval for $|\Delta\mathfrak{L}_{AB}^{\pm}|$ is determined relative to the magnitude of sampled particles, which is achieved by inspecting the delta function $f_{|\Delta_{21}|}$. This function takes in the values of the two cases and subtracts them to see which value is dominant with a high probability to project one of the corresponding measurement outcomes from Eq. (30), in column $\mathfrak{M}(\omega_{|l}, \Delta t^*)$ of the table. In this column, a pairwise interaction is presented in the tensor form $|i_m i_n\rangle$, while for an odd number of particles, e.g., $n = 3$, one of which is a photon interacting with a pair as a direct sum $|i_m i_3\rangle \oplus |1_1\rangle$, Eq. (11). The dominant value

determines the quantum mechanical expectation value for a QDF transformation in the rightmost column. This forms a QPT satisfying a BEC result (potential energy moment) as opposed to an excited state (kinetic energy moment) via $f(\kappa)\rho$ based on Eq. (30). The interval for $|\Delta\mathfrak{L}_{AB}^\pm|$ is the expected concave product $> \frac{1}{2}L_{\mathcal{E}}^{-D}$, and convex product $\leq 0.1L_{\mathcal{E}}^{-D}$ from Table 2, or a combination for particle pairs where EE is encoded. The dominant case in the rightmost column is the result based on the comparison made between the first two columns to show which particle among n particles entangle in a CNOT operation over L_d , Code Listings 1 and 2. This is encoded in layer \mathcal{E} of the quantum circuit, Fig. 6, with a QDF transformation relative to layer \mathfrak{D} . The operators QFT and QFT^{-1} in the QDF operate within the κ -limit, and act on a quantum state. This is a unitary transformation which preserves the inner product $\langle\Psi|\Phi\rangle$ from Eq. (13). Each operator at step s maps superpositions of N states, $\{|0\rangle, |1\rangle, \dots, |N-1\rangle\} \mapsto \{|0_m\rangle, |1_m\rangle\} \rightarrow |i_m\rangle$ via $j \in |ij\rangle \rightarrow |i_m i_n\rangle$, [4, Remark 6], with L_d storables points, see Eq. (30) and Remark 4. As a result, the QDF operator containing both operators QFT and QFT^{-1} , maps superpositions of N states, $\{|0_m\rangle, |1_m\rangle\} \leftrightarrow |i_{ll'}\rangle\Psi(\tau) = |2\rangle\Psi(t) \rightarrow |i_n\rangle$, Eq. (30), where a result of $|i_n\rangle \rightarrow i$ can be decoded at t^* of Eq. (15), from layer \mathfrak{D} of Eq. (35).

The QDF can be expressed as a map of QFT and QFT^{-1} via κ transformation operators as follows.

$$\begin{aligned} \mathcal{E}\mathcal{E}_2(\text{QFT}^{\pm 1}f(\kappa)\rho, s) &= \begin{cases} \mathcal{E}\mathcal{E}_2((\text{QFT})\kappa\Phi, s) : \frac{|i_m i_n\rangle}{\langle\mathbf{r}_{i_{ll'}}|\mathbf{r}_{j_{ll'}}\rangle} \xrightarrow{\kappa\Phi} \lim_{|\mathbf{kr}| \rightarrow 1} \frac{\omega_{|1_m\rangle}}{\sqrt{\langle L_d\rangle}} \sum_{\langle ll'\rangle}^{N=2^{n-1}} \Psi\left(\mathbf{r}_{i_{ll'}}|\mathbf{r}_{j_{ll'}}\right) \omega_{ll'}^{\frac{2\pi}{L_d} i_m i_n} |i_{ll'}\rangle \langle j_{ll'}|, \\ \mathcal{E}\mathcal{E}_2((\text{QFT}^{-1})\kappa^4\Psi^2, s) : |i_{ll'}\rangle \xrightarrow{\kappa^4\Psi^2} \lim_{|\mathbf{kr}| \rightarrow 1} \frac{\omega_{|0_m\rangle}}{\sqrt{\langle L_d\rangle}} \sum_{m,n}^{N=2^n} \Phi\left(\mathbf{k}_{i_{ll'}}|\mathbf{k}_{j_{ll'}}\right) \omega_{ll'}^{-\frac{2\pi}{L_d} i_m i_n} |j_n\rangle \langle i_m|, \end{cases} \\ \therefore \mathcal{E}\mathcal{E}_2(\text{QDF}f(\kappa)\rho, t^*) &\xrightarrow{\Delta t^{*-s}} \mathfrak{D}(|i_m i_n\rangle, t^*) = (\text{QFT})\omega_{|1_m\rangle}(\text{QFT}^{-1})\omega_{|0_m\rangle} \sum_{n=2^0}^{N=2^n} e^{-\beta(E_{i_n} + \sum_n E_{i_n})} \underbrace{\sum_{n=2^0}^{N=2^n} e^{\Delta H^+}}_{\psi_{i_n}(\mathbf{r}, t^*)} |i_n\rangle, \end{aligned} \quad (35)$$

where H^+ satisfies the second condition of Eq. (18) for the spin Hamiltonian in Eq. (36), and the QFT via $\kappa\Phi$ in $\mathcal{E}\mathcal{E}_2$ acts on quantum state $|i_m i_n\rangle$, and \mathfrak{D} acts on its output denoting the binary readout of the compressed qubits, which is the decompressed form of classical bits. The upper-limit of the sum on the QFT side within a QDF transformation is $\langle ll'\rangle \rightarrow |\langle\mu_{ij}\rangle| = N/2 = 2^{n-1}$, for the expected sites $\langle ll'\rangle$ from Eq. (16). This magnitude satisfies the lower-bound of the quantum mechanical expectation value in Eq. (34), under Case 2 of Table 4. For the inverse QFT, QFT^{-1} via $\kappa^4\Psi^2$ from the QDF lens product in Table 1, the pairwise particle interaction becomes $\omega_{ll'}^{-2\pi ij}$, which describes the energy state of photons projecting off of particle sites l and l' . Their energy states are observed via $|i_m\rangle$ and $|i_n\rangle$ in a QDF matrix. The QDF matrix can be constructed by mapping from QFT, $\kappa\Phi$ and QFT^{-1} for each phase shift at a given time step in Eqs. (29)–(35).

```

1 # Quantum simulation of a quantum field lens coding algorithm with entanglement scaling
2 # between multi-well barrier of internal system B and external system A.
3 #
4 #
5 # Import the QISKit SDK
6 import numpy as np
7 from qiskit import QuantumCircuit, ClassicalRegister, QuantumRegister, Aer,
8 execute, IBMQ
9 from math import pi
10 from qiskit.compiler import transpile, assemble
11 from qiskit.tools.jupyter import *
12 from qiskit.visualization import *
13 from ibm_quantum_widgets import *
14 from qiskit.tools.monitor import job_monitor
15
16 # Set your API Token. IBMQ.enable_account ('API Token')Create a Quantum Register with
17 # 4 qubits.
18 q = QuantumRegister(4)
19
20 # Create a Classical Register with 4 bits.
21 c = ClassicalRegister(4) # as _b in Fig. 6
22
23 # Create a Quantum Circuit
24 qc = QuantumCircuit(q, c)
25
26 #-----
27 # Implementation of Superdense Coding
28 #-----
29 # State initialization on 4 qubits in the z-basis in the |0> state.
30 qc.reset(q[0])
31 qc.reset(q[1])
32 qc.reset(q[2])
33 qc.reset(q[3])
34 qc.x(q[0])
35 qc.x(q[2])
36 qc.barrier(range(4)) # Barrier to indicate physical barriers between systems A and B
37 # particles in communication.
38 qc.h(q[1])
39 qc.cx(q[1], q[2])
40 qc.barrier(range(4))
41 qc.z(q[1]) # Current state encoded in the message through QFT.
42 #qc.z(q[1]) # Current message encoded in the superdense coding scheme.
43 qc.barrier(range(4))
44
45 # Time step = 1. Time evolution of potential energy part of the Ising model (spin
46 # configuration tending to ground state or magnetization H>0) relative to kappaPhi
47 # implementation.

```

Listing 2. The QDF lens coding circuit written in OpenQASM 2.0 via IBMQE [64]. The equivalent control- U gate U_3 [76] in QI is the CR_k gate with angle $\theta = \pi/2^k$ radians, which is a parameterized controlled phase shift [64,65]. Download code from [5].

```

48 qc.h(q[2])
49 qc.u3(8,-pi/2,pi/2,q[2])
50 qc.h(q[2])
51
52 #-----
53 # Entanglement Encoder Implementation
54 #-----
55 # Two-qubit Inverse Quantum Fourier Transform (QFT^-1)
56 qc.h(q[1])
57 qc.cu1(pi/2, q[2], q[1])
58 qc.h(q[2])
59
60 # Time evolution of kinetic Ising model (kinetic energy part satisfying magnetization
61 # value M=0)
62 qc.p(pi/2, q[1]) # kappa scalar implementation
63 qc.h(q[1])
64 qc.u3(-(pi**2)/30, -pi/2, pi/2, q[1])
65 qc.h(q[1])
66 qc.h(q[2])
67 qc.u3(-(pi**2)/8, -pi/2, pi/2, q[2])
68 qc.h(q[2])
69 qc.cu1(pi**2)/8, q[2], q[1])
70
71 # Two-qubit Quantum Fourier Transform (QFT)
72 qc.h(q[2])
73 qc.cu1(-pi/2, q[2], q[1])
74 qc.h(q[1])
75
76 # Time evolution of potential energy part
77 qc.p(3*pi/4, q[1])
78 qc.h(q[2])
79 qc.u3(6, -pi/2, pi/2, q[2])
80 qc.h(q[2])
81
82 qc.barrier(range(4))
83
84 #-----
85 # Continuation of the superdense code algorithm. Remove IF statement for real quantum
86 # computers when enabling one of the backends after 'ibmq_qasm_simulator' below
87 #-----
88 qc.x(q[1]).c_if(c, 1) # IF statement, as if the prize is spotted via Eve or the
89 # audience ask Bob to decide to win the prize or a prize of lesser quality or energy
90 # value; flipping condition for Alice to cloak the prize is 0 as opposed to 1 or 2 in
91 # decimal. Remove IF statement when testing on a quantum computer and not a simulator.
92 qc.barrier(range(4))
93 qc.cx(q[1], q[2])
94 qc.h(q[1])
95 qc.barrier(range(4))
96 qc.measure(q[2], c[0]) # Qubit 2 is in state |0>
97 qc.measure(q[1], c[1]) # Qubit 1 is in state |1>
98
99 # Remove IF statement for real quantum computers when enabling one of the backends after
100 # 'ibmq_qasm_simulator' below qc.swap(q[1],q[2]).c_if(c, 1) # SWAP gate is used if
101 # condition c=1 or 01 in binary.
102 qc.swap(q[1],q[2]).c_if(c, 2) # SWAP gate is used if condition c=2 or 10 in binary.
103 qc.measure(q, c)
104 qc.barrier(range(4))
105
106 #-----
107 # Choose backend, number of shots and the plotting of histogram.
108 #-----
109 my_provider = IBMQ.load_account()
110 print(my_provider.backends())
111 ibmq_pick = my_provider.get_backend
112 ('ibmq_qasm_simulator')
113 #ibmq_pick = my_provider.get_backend
114 #('ibmq_athens')
115 #ibmq_pick = my_provider.get_backend
116 #('ibmq_16_melbourne')
117 shots = 8192 # Number of shots to run the program (experiment); maximum is 8192 shots.
118 max_credits = 10 # Maximum number of credits to spend on executions.
119 job_exp = execute(qc, backend = ibmq_pick, shots = shots, max_credits = max_credits)
120 job_monitor(job_exp)
121 result = job_exp.result()
122 counts_exp = result.get_counts(qc)
123 print(result.get_counts(qc))
124 plot_histogram(counts_exp)
125
126 #-----
127 # Visualize the Circuit
128 #-----
129 editor = CircuitComposer(circuit = qc)
130 editor

```

Listing 2. Continued

The kinetic and potential energy operations can be executed from the QDF's first two conditions in Eq. (35). This is based on their coordinate representation by $2n$ -qubit gates in the quantum circuit (lens system).

Remark 6. Extra qubit gates added to $2n$ -qubit gates denote *ancilla* (extra) *qubits* for storing, then training the QF-LCA. This is conducted by a slave particle (see p. 3) to store entangled states and later use this particle to decode in binary for a classical communication [40] between $2n$ particles in the game, see Code Listing 1.

The operations are executed after a small time interval Δt^* , where the system's time evolution [37] is implemented via Eqs. (15) and (35). The potential energy based on state $\Delta E(M > 0)$ in Eq. (30) as $E = N(\hbar c \pi / L)$ is observed by measuring $\omega_{ll'}^{-2\pi i j}$ for a photon produced in a trap, and projected between sites l and l' towards a QPT. This rotation value satisfies an energy phase shift, Eqs. (12)–(19), and (30). The value can be added to the spin Hamiltonian relative to $\kappa\Phi$ or $\kappa^2\Psi$ transformation in Eq. (35). This transformation, expectedly shifts all of the energy eigenvalues for a $\Psi(t \mapsto \tau)$ in the quantum circuit, by an amount of

$$H\Psi(t \mapsto \tau) = \overbrace{E\Psi + \Delta E\Psi}^{\Delta H^+\Psi} = \left(E_{i_n} + \sum_n^N E_{i_n} \right) |\Psi_{i_n}\rangle. \quad (36)$$

The expected energy value from a QDF transformation and the decoder \mathfrak{D} from Eq. (35) is reflected in Table 4. This condition $H\Psi = \Delta H^+\Psi$ satisfies the second condition in Eq. (18), which describes a photoprobe reading a BEC and its formation in a trap

Table 4

Expectation values of EE in [Table 2](#) to implement a QDF circuit. The results have been extrapolated from the data presented in [Fig. 6](#), which correspond to [Eq. \(32\)](#). The expected probability of a qubit state in binary is $P_{|ij\rangle} \geq 2/3$ for $\underline{b}(|ij\rangle)$ in the rightmost column, which denotes superposition, entanglement or a classical state for a particle (qubit) pair. The expected probability $P_{|ij\rangle} \geq 2/3$ is $\underline{b}(01) = 1$ or $\underline{b}(0 \leftrightarrow 0_m 0_n) = \{0, 2\}$, and its complement on both outcomes $P'_{|ij\rangle} = P_{|11\rangle} \leq 1/3$, is $\underline{b}(11) = 3$, according to [Figs. 6\(b\)](#) and [6\(c\)](#). This is measured alongside a photoprobe state projected onto the excited state $|1\rangle$ of the qubit pair. This projection is observed between pairwise particles as their states are registered by qubit registers q_1 and q_2 , according to [Fig. 6](#). These states are separable for a prediction based on a particle-pair energy measurement $\mathfrak{M}(\omega_{|ij\rangle}, \Delta t^*)$, projecting the expectation values of ΔH^+ and M . The expected kinetic and potential energy between particles can be measured by comparing the intervals projected for $|\Delta \mathfrak{L}_{AB}^\pm|$ in [Table 2](#) with its expected value $\langle |\Delta \mathfrak{L}_{AB}^\pm| \rangle$. This is computed between lensing events as well as entanglement, given the correlation $\langle kr \rangle$, particle interaction factor, and L relative to d , as discussed since [Eq. \(9\)](#) and [Table 1](#). The expected measurement outcome $\langle M \rangle$ is based on $\langle \Delta H^+ \rangle$ and the events observed in [Fig. 6](#). On a micro-level observation, these results focus on probability values $\geq 2/3$ for a decision point to be made based on $|ij\rangle$ values in binary \underline{b} , given $|i_m\rangle$ and $|i_n\rangle$. On a macro level, the micro-observation results correlate with $|\Delta|_{A:B=B:A}$ calculations (of $|\Delta|$ results in [Table 2](#)), which determine the thermodynamic process to be reversible, $A : B = B : A$, else, irreversible $A : B \neq B : A$. This process estimation (or classification via [Eq. \(37\)](#)) is based on $\langle |\Delta \mathfrak{L}_{AB}^\pm| \rangle$ determined between systems A and B relative to L_ε . The results between columns $|\Delta|_{A:B=B:A}$ and $\langle M \rangle$, positively correlate and indicate which area site is zero, para, ferromagnetic or anti-magnetic [Fig. 3](#), within the corresponding intervals, relative to the expectation values projected for \mathfrak{M} and ΔH^+ . An extensive representation of the table with QFT, QFT^{-1} and QDF moments, according to EE scaling can be derived from the rightmost column, given the quantum lens distance-based classification, which satisfies a QAI technique [\[42\]](#).

n	Case 1: $\langle \Delta N \rangle = \mu_{ij}$ for $ \{\mu_{ij}\} $	Case 2: $\langle \Delta N \rangle < \mu_{ij}$ for $ \{\mu_{ij}\} $	$f_{ \Delta_{21} }$	$\langle \Delta \mathfrak{L}_{AB}^\pm \rangle$	$ \Delta _{A:B,A}^{B,A}$	$\mathfrak{M}(\omega_{ ij\rangle}, \Delta t^*)$	$\langle \Delta H^+ \rangle$	$\langle M \rangle$	$\langle \mathfrak{M}(\mathcal{P}, \psi_{ij}) \rangle = \left\{ \begin{array}{l} \mathfrak{P}_{ ij\rangle} \geq \left \sqrt{\frac{2}{3}} ij\rangle, \mathcal{P}'_{ ij\rangle} \right\} \underline{b}(ij\rangle) \end{array} \right.$
1	$1/\sqrt{2}$	$\{[1/\sqrt{2}, \sqrt{2}], n+1=2\}$	$\{[0, 1/\sqrt{2}], 1, 3\}$	$< \frac{1}{3} L_\varepsilon^{-D}$	0	$ 1\rangle \rightarrow 1\rangle$	E_{11}	0	$\underline{b}(11) = 1$
2	1	[1.5, 3]	[.5, 2]	$\leq L_\varepsilon^{-D}$	≥ 0	$ i_m 0_2 \rightarrow 2\rangle$	ΔE	≥ 0	$\underline{b}((00, 10) = \{0, 2\})$
3	1.22	[1.63, 4]	[.4, 2.78]	$\leq L_\varepsilon^{-D}$	≥ 0	$\{i_m 0_3 \oplus 1_1\rangle\} \rightarrow 2\rangle \oplus 1_3\rangle$	$E_{13} + \Delta E$	≥ 0	$\underline{b}((00, 00 + 10, 1) = \{(0, 2), 1\})$
4	$\sqrt{2}$	[1.767, 5]	[.35, 3.5]	$> \frac{1}{2} L_\varepsilon^{-D}$	> 0	$\{i_m 0_2 0_3 0_4\} \oplus \{[1_1], [1_{n-1}] \} \rightarrow 1\rangle \oplus 0\rangle \oplus 1_{n>1}\rangle$	$\frac{1}{2}(E_{11} + E_{1_{n>1}}) + \sum_n^4 E_{0_n}$	> 0	$\underline{b}(((0, \mathcal{E}(\{10, 00\}) \xrightarrow{\text{swap}} \{01, 00, 0\}), 1), 1) = \mathfrak{D}(\{01, 10, 01\}, t^*) = \{\mathcal{P}_{(01)} \underline{b}(01), \mathcal{P}_{(11)} (\underline{b}(10) + \underline{b}(01))\} = \{1, 3\}$
5	1.58	[1.897, 6]	[.31, 4.42]	$> \frac{1}{2} L_\varepsilon^{-D}$	> 0	$\{i_m 0_2 0_3 0_4 0_5\} \oplus \{[1_1], [1_{n \pm 1}] \} \rightarrow 1\rangle \oplus \bigoplus_n^5 0_n\rangle \oplus 1_{n>1}\rangle$	$\frac{1}{2}(E_{11} + E_{1_{n<n>6}}) + \sum_n^5 E_{0_n}$	> 0	$\underline{b}(((0, \mathcal{E}(\{10, 00, 0\}) \xrightarrow{\text{swap}} \{01, 00, 0\}), 1), 1) = \mathfrak{D}(\{01, 00, 10, 1\}, t^*) = \{\mathcal{P}_{(01)} \underline{b}(01), \mathcal{P}_{(11)} (\underline{b}(10) + \underline{b}(01))\} = \{1, \{2, 3\}\}$
6	$\sqrt{3}$	[2.02, 7]	[.28, 5.27]						
7	1.87	[2.1, 8]	[26, 6.13]						
8	2	[2.25, 9]	[.25, 7]						
9	2.12	[2.357, 10]	[.237, 7.88]						
10	$\sqrt{5}$	[2.46, 11]	[.224, 8.76]						
\vdots	\vdots	\vdots	\vdots					\vdots	\vdots
N	$\sqrt{N/2}$	$< \infty$	≥ 0	L_ε^{-D}	$f_{ \Delta_{21} } \log_2 \frac{\log 3}{2}$ ≥ 0	$\{i_m 0_2 \dots 0_N\} \oplus \{[1_1], [1_{N \pm 1}] \} \rightarrow 1\rangle \oplus \bigoplus_n^N 0_n\rangle \oplus 1_{n>1}\rangle$	$\frac{1}{2}(E_{11} + E_{1_{n<n>N+1}}) + \sum_n^N E_{0_n}$	≥ 0	$\langle \mathfrak{M}(\mathcal{P}, \psi_{ij}) \rangle = \{1, \{2, 3\}\}$

within the system's CNT layer. The encoding-decoding layer, \mathcal{ED} from [Eq. \(35\)](#), builds the physical multi-well (trap) barrier in [Fig. 1\(g\)](#), and complements the circuit representing the quantum lens algorithm as our circuit model below.

Remark 7. The number of matrix elements in [Eq. \(29\)](#) increases proportional to the expansion of the QDF circuit. This is based on sampling and processing more particles with 2^n qubit states, see [Eq. \(35\)](#) and [Table 4](#).

Remark 8. For $2n$ particle sampling and quantum measurement via a particle trap, the propagation of $\Psi\Phi$ in [Eq. \(31\)](#), and $\mathfrak{L}^+(N)$ from [Table 1](#), can scale to a three-particle interaction phase within system B . This is achieved by squaring Ψ as $\langle \Psi^2 \rangle$ via $f(\kappa)$ as [Eq. \(8\)](#), to observe an entangled EPR pair in a QDF, upper [Fig. 1](#). Here, [Eq. \(35\)](#) or [\(36\)](#) energy conditions and phase shifts must satisfy $|\langle \Phi\Psi \rangle| = 1$ for $\Phi\Psi^2 \rightarrow |\langle \Phi\Psi \rangle| \Psi = e^{i\mathbf{k}\mathbf{r}} \sqrt{L^{-3}}$.

As shown in Code [Listing 2](#), different layers are commented on the circuit operators to denote events between systems A and B , relative to EE between particle pairs. The lens coding layer represents the events of [Fig. 6](#) circuit and its outcome, where different QDF operations on qubits can be coded and classified based on [Eqs. \(29\)–\(35\)](#) and [Table 4](#) expected results. The EE measurement components are observed between circuit measurement points (steps) of [Algorithm 1](#). The results of an EE measure are presented in [Fig. 6\(a\)](#), and discussed in Meth. Valid. II as (b)A–(b)F. A magnetization of $M \geq 0$ (BEC), according to [Fig. 3\(c\)](#), can be interpreted as a prize win by Bob predicting a prize state, as the BEC complement (ES), flipped by Alice or any other possible measurement outcome discussed from [Table 3](#) and the QDF circuit.

Quantum lens distance-based classification

From [Example 2](#) and [Eqs. \(22\)–\(29\)](#), a quantum lens classifier can be formulated. By using this classifier, separable states (or zero superposition) are predicted by controlling qubit rotations and the X operator on a pair of qubits [\[53\]](#). For instance, consider an intelligent decision support system (IDSS) built-in, by classifying a decision coming from Bob and other decisions or suggestions

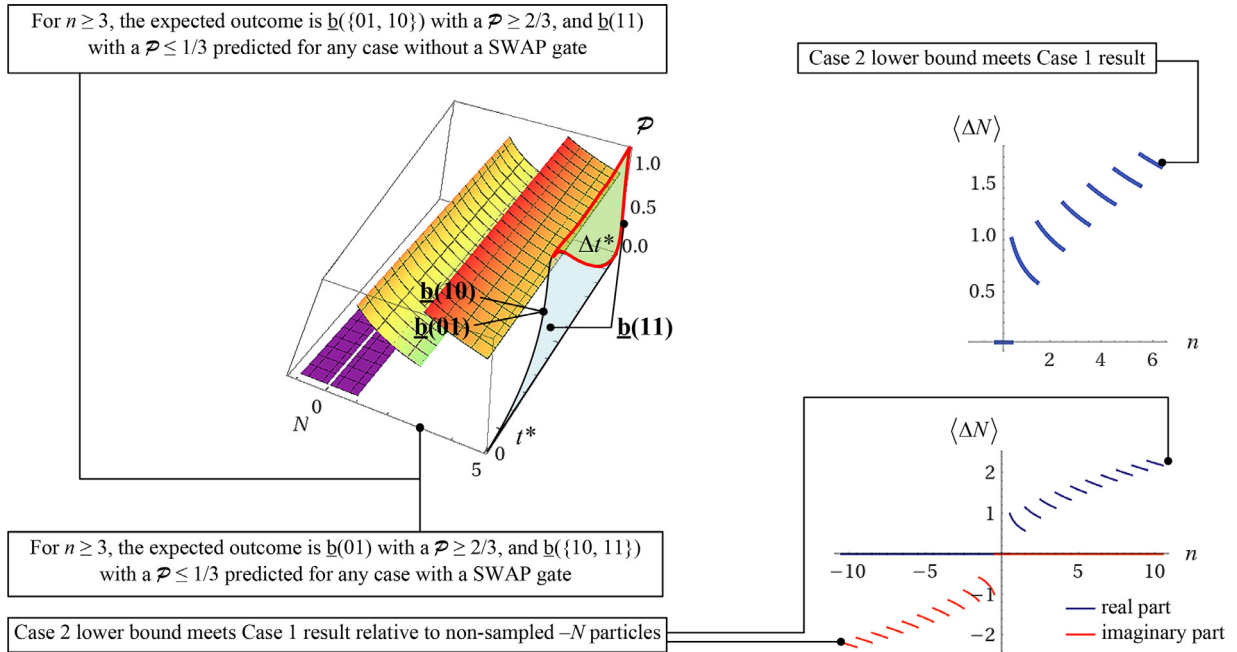


Fig. 7. The EE scaling graphs of the QDF circuit. Left graph illustrates the phase shift region of pairwise particle interactions where the desired Hamiltonian occurs for the expected measurement outcome as shown in Table 4. Each phase shift is time(step)-dependent encoding and decoding in a QDF transformation. The binary string outcomes are predicted as the spin Hamiltonian evolves within the probability density region, or areas of P^{*} . The constant trend with probability $P \leq 1/3$ is for $b(11) = 3$ in decimal as the complement of $b(01) = 1$ and $b(10) = 2$ in all cases for $n \geq 3$ in the rightmost cells. Implementing the circuit with a SWAP gate against a no SWAP gate projects a probability trend of $P \geq 2/3$. The right upper-graph shows Case 2 lower-bound values from Table 4 meet Case 1 results between ΔN and n parameters. The lower-graph projects values between the same parameters relative to non-sampled, and to be sampled $-N$ particles, from A to B, Fig. 2, Eqs. (32) and (33).

from other game participants (particles). Each participant's suggestion or decision can be classed as an ST. An ST or a spin transition contributes to the creation or rerouting of energy paths, making particles participate in a thermal event (a PT). As a result, a more efficient heat engine is expected relative to the system's entropy, Algorithm 1. For example, compared to efficient QFT algorithms [40] with a complexity of $O(n \log n)$ gates, the lens coding algorithm, according to Tables 2 and 4, approximates the QDF transform to $n \log 3$ on the EE scale, which is more efficient in measuring qubits.

New data are usually classified based on already classified (learned) data. A new data point can be classified by representing all data points as features (characteristics), and compute the distance between the features of the new data point and the features of the learned data points [65]. The new data point is assigned to a label with the shortest distance. The quantum lens products generated from their lens function correspond to thermodynamic events in a QDF observed under the Wick rotation $-i\tau = t \mapsto \tau$. Subsequently, the entropy of a lensing event is measured, and the lens product based on the *inverse distance*, from Table 2, is assigned to a label and a class.

In Code Listings 1 and 2, any event probability is measured based on the QDF lens function. From Table 2, the function generates products P and Q , respectively, with distributions $P_{q\pm}$ and Q_{q+} , and their corresponding entropies. These products and their entropies can be classified to determine the energy output relative to a PT. Let χ be the number of classes which defines a binary (classical data) classification. The bottom register ($c[4]$), also denoted by d_4 in Code Listing 2, can then have $n_\chi = \lceil \log_2 \rceil \chi$ qubits. The algorithm compares this quantity to the number of qubits in a mixed state based on entropy $S(\rho_{AB})$ from Table 2. The algorithm further determines EE and classifies where a PT occurs relative to the distribution of particle states in the system.

The same approach can be applied to Code Listing 1 by adding a classical register to the circuit, and label it accordingly [53,65]. However, due to restrictions to run the program on a 5-qubit IBM chip, the fourth register can be labelled based on Fig. 4 circuit configuration [52,53,65]. For more classes, only the n_χ qubits in the classical register need to be set to a state depending on the corresponding class defined below. This can be done using CNOT operations, with control in the first register. A CNOT operation is used to set the label in the bottom register for each data point representing a probability value, given the amount of shots. A test point can be proposed with an inverse distance, which is determined by calculating one of its averages as follows.

$$d_{\{0,1\}}^{-1} = \begin{cases} \langle d_0^{-1} \rangle \xrightarrow{\chi_0} |\Delta \Omega_{AB}^\pm| \leq \frac{1}{3} L_{\mathcal{E}}^{-D}, \text{ for } \xi_0 d_0^{-1}, \\ \langle d_1^{-1} \rangle \xrightarrow{\chi_1} |\Delta \Omega_{AB}^\pm| > \frac{1}{2} L_{\mathcal{E}}^{-D}, \text{ iff } \xi_1 d_1^{-1} < \xi_0 d_0^{-1}. \end{cases} \quad (37)$$

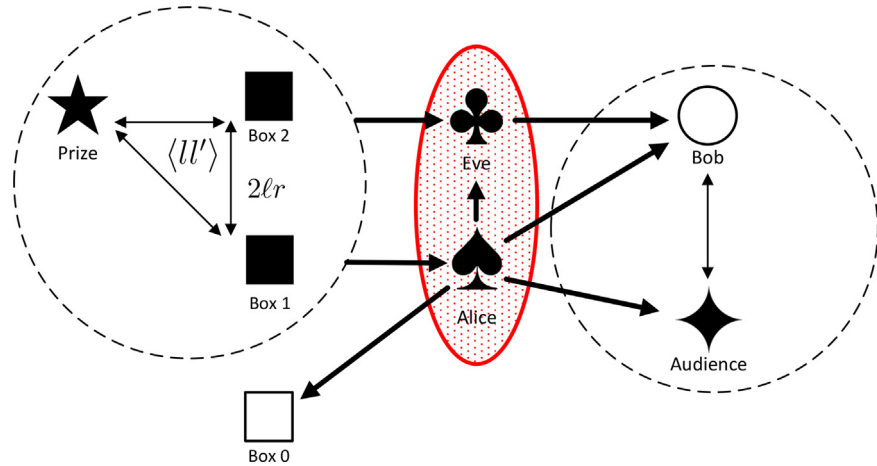


Fig. 8. Left: shows the game steps involving the prize state teleportation between the two remaining boxes after an EPR pair entanglement. The expected area of pairwise interactions $\langle ll' \rangle$ can include the prize state entangled with Alice or Eve when performing Bell measurements across $2\ell r$, Eqs. (25)–(27). Middle: the vital participant in the game circled in red to reveal the hidden information as an extra qubit according to the QDF circuit and transformation. The empty box \square has already been revealed by Alice. Right: Audience \blacklozenge and Bob \circ interacting with game participants in the middle circle relative to the events about the prize on the left. (For interpretation of the references to colour in this figure legend, the reader is referred to the web version of this article.)

The average inverse distance $\langle d_0^{-1} \rangle$ assigns a convex point projection (according to Table 2) as a lens product to class χ_0 with weight ξ_0 , whereas $\langle d_1^{-1} \rangle$ assigns a concave lens product to class χ_1 , with weight ξ_1 . This distance is given the first label, only if $\xi_0 d_1^{-1} > \xi_1 d_0^{-1}$. Conversely, this inverse distance measure can also be used to solve the problem of classes with different number of data points, as discussed in [53]. Any other combination of a convex and concave lens product can be used as a data reference point assigned to the corresponding class.

Remark 9. The reason for having average inverse distances is to average out the macro and micro-level observations of particle states evident from the data points assigned to a class. This method is applied during the field lens coding process between systems A and B . The average distance is measured relative to its specific weight, expecting a PT by analyzing data from the qubit registers.

Labels construct data points denoting the probability distribution obtained by the QF-LCA. This is done by a number of gates where the assignment of indices to data points is made. For instance, suppose the following four indices encode and register quantum states as $|00\rangle$, $|01\rangle$, $|10\rangle$ and $|11\rangle$ with two classes. A single CNOT operation is required for assigning $|10\rangle$ and $|11\rangle$ to class χ_1 , with the most significant qubit as control.

A classifier can be prepared (as discussed in [52,53]) between two registers, where qubits are superposed and entangled during the encoding process, as outlined in Figs. 4–6. A trainable algorithm can have two Hadamard operations [53,65] which sets the first two registers to a uniform superposition.

Class χ_0 : States $|000\rangle$ and $|001\rangle$ set by initialization. The prize is in a BEC state (rightmost qubit or the least significant qubit) as Alice maintains a hidden state $b(0)$ of the prize (leftmost qubit or the most significant qubit) against Bob. This state can be expressed as $|0\dots22\dots0\rangle \leftrightarrow |2\rangle$ from Eq. (21), and Fig. 5(b)E's, Meth. Valid. II;

Class χ_1 : States $|010\rangle$ and $|011\rangle$ set by CNOT with target on second qubit, control on the rightmost qubit;

Class χ_2 : States $|100\rangle$ and $|101\rangle$ set by CNOT with target and control on the leftmost qubit;

Class χ_3 : States $|110\rangle$ and $|111\rangle$ set by the two CNOT gates used for Labels 1 and 2.

The above-mentioned states correspond to the index of a state, hence the first register. The bottom register containing the labels in this case is a two-qubit register initialized in $|00\rangle$. To change this to Label 1 ($|01\rangle$) set for class χ_1 , a CNOT is applied with target on the rightmost qubit, and control on the second qubit of the first register (i.e., of the states shown). For Label 2 ($|10\rangle$) set for class χ_2 , a CNOT is used, but now target on the leftmost qubit in the bottom register, and control on the leftmost qubit in the first register containing the indices. By combining these two operations, the label is set for class χ_3 . The main idea is to re-index the quantum states to minimize the number of operations for setting the labels.

The Code Listing 2 circuit can provide a decision point based on the label value generated by an IF-statement function. This function satisfies both, the class and label values in constructing an IDSS. Therefore, Bob versus Alice conditionally decides to change and/or observe energy states in the game. Note that, this function is available in quantum simulators, but not available on real quantum computers yet, [64].

Example 5. A low probability of an event in Figs. 6(a) $\mathcal{E}\mathcal{E}_2$ -left, and 6(a) $\mathcal{E}\mathcal{E}_2$ -right, is the binary string $b(11) = 3$ in decimal as the prize state to remain in superposition (or unknown) to Bob and Eve, Table 5. These two observe the event at Bob's decision point which results in Bob's win or loss. Alice maintains a box with no prize $b(00) = 0$ against $b(01) = 1$ or $b(10) = 2$, respectively, as outputs

Table 5

Upper table: Corresponds to [Table 1](#) expected measurement outcomes. To predict these outcomes with certainty, qubits are constructed in the third column with eliminable three and four states from [Eq. \(26\)](#), distinguishing Bell states in the QDF circuit given N participants. Using the assigned character set notations from [Eq. \(26\)](#), one participant is vital to reveal the hidden information about the prize to any other participant, as a predicted measurement outcome shown in upper [Fig. 1](#). **Lower table:** Distinguishes states from lens products without entanglement that mimic Bell states in the upper table using an extra qubit which denotes the vital participant who can reveal the hidden information, according to [Eq. \(27\)](#). This table denotes the recorded \mathcal{P} 's as in [Fig. 7](#) and [Table 4](#), by implementing a SWAP and no SWAP gate in the QDF circuit, resulting in separable and orthogonal states.

$ i_m\rangle$ via $j \in$ $ ij\rangle \rightarrow i_m i_n\rangle$ measurement	Pairwise state $\Theta(2\ell r)(0_m i_n\rangle \pm 1_m i'_n\rangle)\spadesuit \circlearrowleft$	Box prize state $ i_m\rangle$; particle example; vital particle box with prize; remaining box is 0 prize \square ; \clubsuit is vital to \circlearrowleft	State type distinguished Bell states
$ 1\rangle$ via $ 12\rangle$	$\otimes 22\rangle \clubsuit$ $\Theta(2\ell r)(0_m 0_n\rangle - 1_m 1_n\rangle)\spadesuit \circlearrowleft$	prize suggested to \circlearrowleft ; \circlearrowleft predicts 0; \clubsuit can reveal hidden information	Bell state
$ 0\rangle$ via $ 01\rangle$	$\otimes 02\rangle \clubsuit$ $\Theta(2\ell r)(0_m 1_n\rangle - 1_m 0_n\rangle)\spadesuit \circlearrowleft$	prize is entangled with \circlearrowleft or \clubsuit ; \clubsuit via \clubsuit is vital to \circlearrowleft	Bell state
$ 1\rangle$ via $ 11\rangle$	$\otimes 22\rangle \clubsuit$ $\Theta(2\ell r)(0_m 1_n\rangle - 1_m 0_n\rangle)\spadesuit \circlearrowleft$	0 prize is entangled with \circlearrowleft or \clubsuit ; \clubsuit is vital to \circlearrowleft	Bell state
$ 0\rangle$ via $ 00\rangle$	$\otimes 00\rangle \clubsuit$ $\Theta(2\ell r)(0_m 0_n\rangle + 1_m 1_n\rangle)\spadesuit \circlearrowleft$	prize is in superposition: poor or else; a bit pair about \star is hidden	Bell state
$ 0\rangle$ via $ 02\rangle$	$\Theta(2\ell r) 22\rangle \spadesuit \circlearrowleft 2\rangle \star$	prize is hidden while \circlearrowleft decides	One pair of states indistinguishable
$ 1\rangle$ via $ 10\rangle$	$\Theta(2\ell r) 21\rangle \spadesuit \circlearrowleft 2\rangle \star$	prize is hidden while \circlearrowleft finds it; \clubsuit is vital to \circlearrowleft	One pair of states indistinguishable
$ 1\rangle$ via $ 10\rangle$	$\Theta(2\ell r) 21\rangle \spadesuit \circlearrowleft 22\rangle \clubsuit$	Distinguished without entanglement	
$b(ij\rangle)$	Distinguishing without entanglement	QDF bits of information; a box prize state out of three known?	State preserved
$b(00) = 0$	$\Theta(2\ell r) 0_m\rangle \spadesuit 0_n\rangle \circlearrowleft 0_{uv}\rangle \clubsuit$	$ 0\rangle 0\rangle$ 1b; Yes, if \clubsuit reveals \square	$ \square\rangle = 0$ by \spadesuit
$b(01) = 1$	$\Theta(2\ell r) 1_m\rangle \blacksquare 2\rangle \spadesuit 2_{uv}\rangle \star 2\rangle \clubsuit$ $\Theta(2\ell r) 2\rangle \blacksquare 1_n\rangle \circlearrowleft 2_{uv}\rangle \spadesuit$	$ 0\rangle 0\rangle$ 1b; Yes, if \spadesuit reveals \star	$ \blacksquare\rangle = \{1, 2\}$ without a SWAP gate
$b(10) = 2$	$ 2\rangle \{\clubsuit, \star\}$	$ 0\rangle 1\rangle$ 1b; Yes, if $\{\clubsuit, \star\}$ reveals \star	$ \blacksquare\rangle = 1$ with a SWAP gate by \spadesuit
$b(11) = 3$	$\Theta(2\ell r) 2\rangle \spadesuit 2\rangle \circlearrowleft 1_{uv}\rangle \star 2\rangle \clubsuit$	$ 0\rangle 1\rangle$ 1b; Yes, if \clubsuit reveals \star to \circlearrowleft	$ \star\rangle = 2$ entangled with \spadesuit or \circlearrowleft

$b(00 + 01) = 1$ and $b(00 + 10) = 2$ between the two remaining boxes. If Eve shares information about the prize based on the average inverse distance values from [Eq. \(37\)](#), Bob will then have a picture for where the prize is. He can have his state entangled with an expected prize state in the proposed position by knowing the length value of $L_{\mathcal{E}}$. Therefore, the sum of values in decimal are assigned to Classes $\chi_0 - \chi_3$, which correspond to the number of CNOT operations needed and remain consistent between the circuit's encoding \mathcal{E}_1 and decoding \mathfrak{D} layers.

Notably, the amount of information between pairwise qubits during CNOT operations increases, which denotes more uncertainty of the prize state when all qubits are in state $|1\rangle$. When two qubits are paired sharing each other's information via their two-qubit Bloch spheres [13,35], one qubit state becomes more predictable. This is achieved by a rotation about the z -axis (R_z gate), which denotes superposition between a qubit and the qubit representing the prize state, which is projected in the direction of a definite position. The spheres are entangled if $|\langle \mathfrak{P} \rangle|^{\frac{1}{2}} = |\langle \mathbf{r}_{i_{ll}}, \mathbf{r}_{j_{ll}} \rangle|^{\frac{1}{2}} > 1$, whereas separable states or zero superposition is expected once $\mathbf{r}_{j_{ll}}$ is predicted via κ , as $|\langle \mathfrak{P} \rangle|^{\frac{1}{2}} \rightarrow 1$, see upper [Fig. 1](#). Hence, training an algorithm to make a decision becomes less complex when the distribution of states is done through a QDF. This training is satisfied by referring to the information about ES or GS spin configuration from N -qubit states, which are points on a Bloch sphere projected from the QDF.

The information on an energy state can be encoded in phase shifts or qubit rotations. For example, to construct R_x by using three R_y rotations, two of which are controlled to encode a set of data points. These data points can be flipped spins for each class, or a targeted basis state of e.g., z -basis $\{|0\rangle, |1\rangle\}$ of a qubit Bloch sphere. This rotation value satisfying an energy phase shift can be added to the system Hamiltonian, [Eq. \(36\)](#), or applied in the interaction Hamiltonian to create an entangled BEC EPR pair, [Eq. \(17\)](#). For encoding, the angle of qubit rotation maps to a thermodynamic event based on $t \mapsto \tau$ under a Wick rotation, [Eqs. \(12\)–\(19\)](#).

In the QF-LCA learning process, the expected values of ΔN relative to n in [Table 4](#) need to be averaged out with the number of entangled and superposed two-qubit spheres. This is to make strong predictions of the prize state, and thereby make a decision by which the amount of entropy decreases to near 0 values.

Method validation - Part II

In [Figs. 4](#) and [5](#), the algorithm implements a QFT within a κ -based QDF transformation, as a single step between the energy input side and the energy output side of the system. The following outcomes were observed from the order of events in [Fig. 5\(b\)](#):

5(b)A. A quantum outcome based on a κ -based QDF transformation scenario: a QFT followed by its inverse in two iterations, via $\kappa\Phi \rightarrow \kappa^{-2}\Phi\ell r$, [Eq. \(8\)](#), was observed with no SWAP gate.

5(b)B. A quantum outcome having the SWAP gate compared to outcome 5(b)A.

- The outcome is for two tries of Bob to win the prize (playing the game twice) by running the adder subcircuit `.full_adder` twice as `.full_adder(2)`.
- The inclusion of the latter outcome with the `.full_adder(1)` outcome, returns the likely outcome 000110b or 010010b, with a probability $\geq 1/2$. This maps to a high probability of Bob winning the prize with a SWAP gate.

5(b)C. Optimised (a classical deterministic outcome).

5(b)D. –F. Alice against Bob maintains a high probability of a state $|0\rangle$ outcome between all boxes hiding the prize via superposition and entanglement as e.g., an entangled BEC EPR pair from [Example 2.B](#), until Bob makes a decision. This is expressed as the binary string $000000b \rightarrow |2\rangle$ for an initialized game step.

- This outcome is achieved by changing the number of iterations of subcircuit `.sender_encode_bits(1)` to (2).
- Given the game steps and its outcome, changing the number of iterations of subcircuit `.receiver_decode_bits(1)` to (2) alongside `.sender_encode_bits(2)` (other sub-circuits have iteration (1)), reduces the likelihood of Alice's success against Bob's win at decision point to $P' \leq 1/3$, with or without the SWAP gate. The outcome is 010110b, which is the complement of the high probability in [Fig. 5\(b\)E](#), for Bob to win the prize with a $P \geq 2/3$ (as counted by the adder). A probability ≈ 1 with no SWAP gate returns 000010b, see [Fig. 5\(b\)F](#) results.

The expansion of the quantum circuit is illustrated in [Fig. 6\(a\)](#), which is a QDF transformation that maps to \mathcal{EE}_2 after superdense encoding \mathcal{E}_1 . The expected values for entanglement scaling are reflected in [Table 4](#) and discussed in the EE measurement section. The key point from this discussion is that, \mathcal{EE}_2 can be efficiently implemented by determining which one or more groups of particles (such as target qubits) are expected to entangle. This EE scalar behaviour is determined when the results in the table are inspected. The circuits, based on Code [Listings 1](#) and [2](#), can be labelled and implemented for machine learning purposes (the QI version is discussed by [\[53\]](#)), which satisfy the prediction and evolution of energy states in the heat engine, [Eq. \(36\)](#).

The following were observed from [Fig. 6\(a\)](#), corresponding to game event predictions relative to [Eq. \(10\)](#):

6(a) $\mathfrak{D}(\mathcal{EE}_2, t^*) \rightarrow \mathfrak{M}_1 \rightarrow S$:

A quantum outcome from a κ -based QDF transformation scenario: transformation $\kappa\Phi \rightarrow \kappa^{-2}\Phi\ell r$ in a QFT and its inverse was observed in a stepwise time-evolution with or with no SWAP gate (line # 43–80, Code [Listing 2](#)).

6(a) \mathcal{EE}_2 -right:

A simulated IF-statement condition is the prize to be spotted via Eve or the audience: ask Bob to decide and win the prize, or a prize of lesser quality/energy value. This is a QPT or CPT, as shown in [Fig. 6\(a\)](#), corresponding to possible outcomes, one is the flipped condition for Alice to cloak the prize in state $|0 \leftrightarrow 2\rangle$, as opposed to $|1\rangle$, which is $b(10) = 2$ in decimal, [Fig. 6\(c\)](#).

6(a) $\mathfrak{D} \rightarrow \mathfrak{M}_2(|\Delta\mathfrak{L}_{AB}^\pm| > \frac{1}{2} L_{\mathcal{E}}^{-D})$:

An expected outcome as the complement of the output from [Fig. 6\(a\)](#) \mathcal{EE}_2 -right, is $b(01) = 1$ in decimal, where Alice shows Bob an empty Box as 0, as opposed to where the prize is, as 1 in [Fig. 6\(b\)](#).

6(a) $\mathfrak{D} \rightarrow \mathfrak{M}_2(|\Delta\mathfrak{L}_{AB}^\pm| \leq L_{\mathcal{E}}^{-D})$:

A lower probability of either event $\leq 1/3$ in [Fig. 6\(a\)](#) \mathcal{EE}_2 -left, and [Fig. 6\(a\)](#) \mathcal{EE}_2 -right, is $b(11) = 3$ in decimal. This is the prize state to remain in superposition relative to Bob and Eve's observation at Bob's decision point (the prize is entangled with Bob or Alice). This can result in Bob's win via Alice, $|1_m\rangle$ via $j \in |ij\rangle \rightarrow |1_m 1_n\rangle$, else Alice maintains a box with no prize $b(00) = 0$ against $b(01) = 1$ or $b(10) = 2$, respectively, as output $b(00 + 01) = 1$ or $b(00 + 10) = 2$ between the two remaining boxes, [Tables 4](#) and [5](#).

On an IBM 5-qubit machine (selected from one of the IBMQ back-end providers in Code [Listing 2](#)), with phase gates, and no IF-statements or SWAP gates, the expected probability is ≥ 0.5 for $p(0101b)$ from the binary set $\{p(0101b) + \{p(0100b), p(0001b)\}, p(0011b)\}$. This is obtained from the observations made on the probability distribution spread to other possible binary outcomes after 8192 shots, [Fig. 6\(b\)](#). This is the number of iterations made at time t from Δt^* , which evolves into a number of PT loops, Eq. (15). On the same machine, with a SWAP gate, the expected probability is $\geq 2/3$ for a $p(0011b) + \{p(0001b), p(0010b), p(0111b)\}$ in [Fig. 6\(c\)](#). In both expected outcomes, with the exception of $p(0011b)$ in [Fig. 6\(b\)-right](#), and $p(0111b)$ in [Fig. 6\(c\)-right](#), the probabilities from the machine's lists, respectively, cumulate to $p(0011b)$ and $p(0101b)$ of the simulation results, [Figs. 6\(b, c\)-left](#). This is due to all binary strings map to the same expected outcome in the game with a SWAP gate, when a classical bit is set to $b(10) = 2$. This highlights the importance of implementing components $\kappa\Phi$ and $\kappa^2\Psi$ in a QDF transformation, [Eq. \(35\)](#), using phase gates relevant to QFT^\pm energy components in the circuit.

In Code [Listing 2](#), a symmetric QDF adder can be implemented by adding a `.pre_full_adder` code before line # 37, identical to the sub-circuit `.full_adder` of Code [Listing 1](#). This circuit returns a binary string 010001b with a probability of 0.98, which is the complement of the expected result in [Fig. 5\(b\)C](#), or [Fig. 5\(b\)F](#). From the left part of the string, 01, is for counting the *ancilla qubits* [\[70\]](#), relative to a QDF transformation. These extra qubits can act as a probe to store entangled states, or used for QF-LCA training and error correction. This is by coupling with the energy operator from the QDF transform, as the extra information from these qubits are collected by e.g., Eve, to analyze and share the useful bit (prize state) with Bob. The remaining part of the string, 0001, denotes the NOT gate output via an *X*-gate. This overall outcome shows how the original circuit is formed, and masks any possibilities of post and middle-qubit flips between sub-circuits `.superpose_entangle` and `.receiver_decode_bits`. The exception is that,

the information collected on the prize position is for specific parties, like Alice and Eve with complementary states to distinguish entangled states during the game, Eq. (27).

The same logic applies to the construction of a QDF circuit. The more iterations the system is assigned to perform a quantum computational task, the more accurate the expected value of the energy output denoting a PT, system temperature, or magnetization between particle sites. The time step evolution is evaluated under the Wick rotation to show system temperature change, as the system state evolves over time. An ST can be determined between systems A and B by implementing a $\text{QFT} \leftrightarrow \text{QFT}^{-1}$ operation within the system code. This operation has QDF parameters whose values are generated from circuit components defined as a κ -based QDF transformation. This is where classical data is encoded into a quantum state as an encoding step $\mathcal{EE}_2(\text{QDF}f(\kappa)\rho, t^*)$. In this step, the data on events can be collectively recorded and weighed with distances between data points as discussed and exemplified in the QDF circuit section. The next step is constructing a distance-based classifier to train and determine which quantum circuit component is most likely to generate an ES or a GS in the system. The final step is decoding $\mathfrak{D}(\mathcal{EE}_2, t^*)$ as the output data, which is converted to classical data, Table 4. A QAI leading to a decision-making outcome is achieved after executing these steps [44,54,74].

Conclusion

In this paper, a double-field computation (DFC) model is presented to simulate quantum observations on particle states and their distribution as lens products, which are delivered through quantum lenses in a proposed thermodynamic system. The DFC algorithm simulates and predicts the impact of lens products in the system. These products come from micro-observables, e.g., particles interacting via a quantum double-field (QDF) lens in a quantum phase transition (QPT). The simulated system is split into A and B , where A has particles sampled by B as a heat engine to satisfy a quantum measurement. The algorithm simulates the creation of counter particles by photoprobes, given the energy level change of atoms within B 's physical media. The simulated system has carbon nanotubes (CNTs) obeying the Ising model, and (super)conductors to manifest entanglement contained within the QDF using field lenses that distribute particle states between A and B . Photoprobe fields are generated from the CNTs and the photons from their probe's field are projected onto atomic sites from A , where atoms are sampled and processed in B . Photodetectors gather information from photons that are re-emitted from the atoms to determine their states, prior to a QPT or classical PT (CPT). These thermodynamic events were presented as a QDF circuit, which are referred to quantum operations of the DFC algorithm.

An analysis of the observable particle states was conducted by simulating the distribution of states as lens products, which were projected from one or more lenses over a lens distance as a metric. This included simulating an energy surface contour model to show the magnitude of events, given the lens distance on a micro-level from our lens coding examples. From the lens coding method and metric, a particle state can be determined, predicted, and controlled prior to a PT. For instance, a PT was characterized and predicted by measuring the position-momentum correlation, and the probability of the states distributed under a κ -based QDF transformation via scalar function $f(\kappa)$, from one particle site to another. The distance comparisons made between particle states is a useful metric to show where energy paths behave as BEC atoms in a QPT, otherwise behave in a disordered state with an increased entropy in a CPT. This is done by mapping the correlation length to the upper and lower bounds of κ^2 associated with the probe's superposed field paired with an atomic field, by which get entangled according to the QDF model. This model was originally proposed in form of a quantum game theory model [4], having characters in the game who interact to win a prize of great value which in turn increases entropy as a CPT. However, to win a prize with poor value or a no prize state is a QPT. The summary of game events, such as observing characters who play the role of particles in a ground state (GS) or excited state (ES), is presented to validate the κ -based QDF transform applied to the QDF circuit. Examples such as a BEC production, BEC EPR pairs from a splitting BEC into two traps denoting an entangled prize state with one of the characters or with its split state in a GS, have been simulated and discussed in the current paper.

Furthermore, entanglement length and its divergence between two lensing events relative to their lens distance are observed and analyzed at the PT level. This is done through CNOT lens coding and entanglement entropy (EE) measure based on density matrices and steps to encode and decode states. The keys for this measurement are lenses, photoprobes, photodetectors and a CNOT gate built by contacting CNTs to a superconductor. This is where the number of particle spins is recorded by counter particles once the photoprobes and particles interact. For a high-temperature focused system approaching a CPT, all particles assume a high-energy state. The prediction of slow particles with low-energy states is possible when entangled with high-energy particles by polarized photons through the gate over a lens distance. For a low-temperature focused system approaching a QPT, the converse applies. As the system evolves in its distribution of states, those particles not reaching a desirable state, i.e., the probability of observing a spin up or spin down (GS or ES) outcome at the decoding step, can be rerouted by the heat engine to satisfy a desirable outcome. This establishes a GS or ES energy profile to access and classify states by a classifier. The data points (qubits) in the energy profile are inverse distance-based, and labelled for a specific class. After learning the profile, the classifier decodes and predicts the system state.

The simulated heat engine by the DFC algorithm and its classifier(s) predicts and reroutes particle energy paths on any logarithmic input-output scale. To determine an energy level change in an N -particle system, the QDF lens code or DFC measures EE. The algorithm's classification of EE values determines and distinguishes entangled states in the system. As a result, computations via DFC maximize system efficiency via EE measure on micro and macro levels of energy states distributed in the system. This method can improve quantum computing algorithms to determine which particles participate in a PT, as the next system state evolves and predicted.

Ethics statements

No human participant was involved in the method's data acquisition and analysis.

Declaration of competing interest

The authors declare that they have no known competing financial interests or personal relationships that could have appeared to influence the work reported in this paper.

CRediT authorship contribution statement

Philip B. Alipour: Conceptualization, Methodology, Software, Investigation, Data curation, Writing – original draft, Visualization, Formal analysis, Resources, Funding acquisition, Project administration, Validation, Writing – review & editing. **T. Aaron Gulliver:** Supervision, Resources, Validation, Funding acquisition, Project administration, Writing – review & editing.

Data availability

The data/code used to validate and evaluate our method are within this article. However, any other related links of external data of related articles are provided in the references section.

Acknowledgments

P. B. A. acknowledges Dr. W. Chen endorsement from the Institute of Theoretical Physics at ETH Zürich, for comments on condensed matter physics. P. B. A. also acknowledges the University of Victoria Canada, for financial support. P. B. A. and T. A. G. thank Dr. T. Lu for his comments on the scalar field, dimensions and photonics, Dr. M. Laca for his comments on Eqs. (3)–(10), Dr. N. Neumann remarks from [52–54] on QAI classifiers, and the late Dr. F. Diacu for his input on phase transitions to parameterize their quantum probabilities in the proposed method.

References

- [1] C.M.V. Vliet, Equilibrium and nonequilibrium statistical thermodynamics, WSP, 2010, pp. 5–42, doi:[10.1142/6354](https://doi.org/10.1142/6354). 102, 540, 707
- [2] M.G. Moore, P. Meystre, Generating entangled atom-photon pairs from BEC, Phys. Rev. Lett. 85 (2000) 5026.
- [3] C.H. Wong, et al., Superconductivity in carbon nanotubes and carbyne-nanotube composites, Elsevier BV 125 (2017) 509–515.
- [4] P.B. Alipour, T.A. Gulliver, Quantum double-field model and application, preprint via PHYSO-EM, Elsevier BV 4233203 (2022) 28, doi:[10.2139/ssrn.4233203](https://doi.org/10.2139/ssrn.4233203).
- [5] P.B. Alipour, T.A. Gulliver, Dataset for quantum double-field model and application, Mendeley Data, Elsevier BV, 2023, doi:[10.17632/gf2s8jkdjf](https://doi.org/10.17632/gf2s8jkdjf). V2⁺
- [6] P.B. Alipour, T.A. Gulliver, A double-field computation model to simulate physical systems, Comp. Models., Comp. Theo. J., CompSciRN, Elsevier BV 4239321 (2023) 25.
- [7] T.K. Hakala, et al., Bose-einstein condensation in a plasmonic lattice, Nat. Phys. 14 (2018) 739–744.
- [8] P.E. Black, D.R. Kuhn, C.J. Williams, Quantum computing and communication, adv. in comp., Elsevier, 2002. Sec. 3.4. <https://www.sciencedirect.com/science/article/abs/pii/S0065245802800079>.
- [9] S. Rastgoo, M. Requardt, Emergent space-time via a geometric renormalization method, Phys. Rev. D 94 (12) (2016) 124019.
- [10] M. Damian, S. Pandit, S. Pemmaraju, Lecture notes in computer science, Springer, 2006. 4305, Secs. 4–5
- [11] P. Frąckiewicz, A.G.M. Schmidt, N-person quantum Russian roulette, Physica A 401 (2014) 8–14.
- [12] Committee on AMO, 2010, *Controlling the Quantum World: The Science of Atoms, Molecules, and Photons*, Chaps. 3, 5–7.
- [13] E. Grubling, M. Horowitz, Quantum computing: Progress and prospects, Natl. Acad. Press, USA, 2019. Chaps. 2–5
- [14] T.F. Zhang, et al., Broadband photodetector based on carbon nanotubes, Sci. Rep. 6 (2016) 38569.
- [15] P. Pessoa, C. Cafaro, Information geometry for fermi-dirac and bose-einstein quantum statistics, Physica A 576 (2021) 126061.
- [16] J.O. Haerter, K. Sneppen, Statistical mechanics, the ising model and critical phenomena: complex physics, Niels Bohr Inst., Denmark, 2017. Chap. 1
- [17] S. Suzuki, J. Inoue, B.K. Chakrabarti, Quantum ising phases and transitions in transverse ising models, Springer, 2013. Chaps. 2, 3, 7, 10
- [18] G. Vidal, J.I. Latorre, E. Rico, A. Kitaev, Entanglement in quantum critical phenomena, Phys. Rev. Lett. 90 (2003) 227902.
- [19] C. Lacroix, P. Mendels, F. Mila, Introduction to frustrated magnetism, materials, experiments, theory, Springer, 2016. Chaps. 1–3, 23
- [20] J. Jing, M. Guidry, L.A. Wu, An anomaly in quantum phases induced by borders, Sci. Rep. 10 (2020) 6934.
- [21] W. Li, et al., Scaling behavior of entanglement in free-fermion systems, Phys. Rev. B 74 (2006) 073103.
- [22] P.A. Belov, A.A. Nazarov, A.O. Sorokin, Numerical determination of the CFT central charge in the site-diluted ising model, J. Phys. Conf. Ser. 929 (2017) 012037.
- [23] X. He, et al., Carbon nanotubes as emerging quantum-light sources, Nat. Mat. 17 (2018) 663–670.
- [24] M. Enríquez, I. Wintrowicz, K.Z. Yczkowski, Maximally entangled multipartite states, J. Phys. Conf. Ser. 698 (2016) 012003.
- [25] Y. Zhuang, et al., High-temperature ferromagnetism of helical carbon nanotubes, AIP Adv. 3 (2013) 052112.
- [26] A. Hamma, W. Zhang, S. Haas, D.A. Lidar, Entanglement, fidelity, and topological entropy in a quantum phase transition to topological order, Phys. Rev. B 77 (2008) 155111. Also, <https://pitp.phas.ubc.ca/confs/qc08/talks/haas.pdf> [Accessed, 2018]
- [27] T. Kuwahara, I. Arad, L. Amico, V. Vedral, Local reversibility and entanglement structure of many-body ground states, Quan. Sci. Tech. 2 (2017) 015005.
- [28] T. Kopp, F.J. Seco, S. Schiller, P. Wölfle, Superconductivity in the single-band hubbard model, Phys. Rev. B. 38 (1988) 11835.
- [29] W.-W. Yang, Y. Zhong, H.-G. Luo, Benchmarking the simplest slave-particle theory with hubbard dimer, Chin. Phys. B, IOP Sci. 28 (2019) 107103.
- [30] S.M. Girvin, K. Yang, Modern condensed matter physics, Cambridge Univ. Press, 2019. Chaps. 3, 7, 8, 17, Appx. F.
- [31] D.G. Angelakis, M. Christandl, A. Ekert, Quantum information processing: from theory to experiment, IOS Press 199 (2006). 109–112, 218–237, 312–320
- [32] C. Beny, S. Vishveshwara, L. Balents, M.P.A. Fisher, Quantum entanglement in CNTs, Phys. Rev. Lett. 89 (2002) 037901.
- [33] F. Mandl, G. Shaw, Quantum field theory, Wiley Press, 2010. 2nd ed., pp. 2–24, 40–97, 110–126
- [34] Z. Nussinov, Macroscopic length correlations in non-equilibrium systems, Nuc. Phys. B 953 (2020) 114948.
- [35] C.-R. Wie, Two-qubit bloch sphere, Phys. 2 (2020) 3, 383–396.
- [36] H.T. Ng, C.K. Law, P.T. Leungn, Quantum-correlated double-well tunneling of two-component bose-einstein condensates, Phys. Rev. A 68 (2003) 013604.
- [37] J. Stolze, D. Suter, Quantum computing, Wiley-VCH, 2004. 1st ed., pp. 1–62, 217, Chaps. 1, 2, 4, 6–8, 10–13
- [38] X.-L. Wang, Y.-H. Luo, H.-L. Huang, et al., 18-Qubit entanglement with six photons, Phys. Rev. Lett. 120 (2018) 260502.

- [39] R. Ionicioiu, Schrödinger's cat: where does the entanglement come from? *Quanta* 6 (2017) 57.
- [40] M.A. Nielsen, I.L. Chuang, *Quantum computation and quantum information*, Cambridge Univ. Press, 2010. Chaps. 1, 2, 11, 12, pp. 97, 136–164, 309–424.
- [41] C.R. Nave, Schrödinger equation and qunatum oscillator, redirected from Phys. World IOP J. (2009). <http://physicsworld.com/a/web-life-hyperphysics> [Accessed, 2018]
- [42] G. Acampora, (EIC), Quantum machine intelligence, Springer 1 (2019) 1–3.
- [43] A.T. Sornborger, Quantum simulation of tunneling in small systems, *Sci. Rep.* 2 (2012) 597.
- [44] A. C-Lieta, J.I. Latorre, D. Goyeneche, Quantum circuits for maximally entangled states, *Phys. Rev. A* 100 (2019) 022342.
- [45] J. Romero, J.P. Olson, A. A-Guzik, Quantum autoencoders for efficient compression of quantum data, *Quantum Sci. Technol.*, IOP Sci. 2 (2017) 045001.
- [46] H. Wang, Quantum algorithm for preparing the ground state of a system via resonance transition, *Sci. Rep.* 7 (2017) 16342.
- [47] M. Hanks, M.P. Estarellas, W.J. Munro, K. Nemoto, Effective compression of quantum braided circuits by ZX-calculus, *Phys. Rev. X* 10 (2020) 041030.
- [48] N. Khammassi, G.G. Guerreschi, I. Ashraf, J.W. Hogaboam, C.G. Almudever, K. Bertels, cQASM v1.0: towards a common quantum assembly language, *Quant. Phys.* arXiv:1805.09607 (2018).
- [49] Y. Wang, Z. Hu, C. Sanders, S. Kais, Qudits and high-dimensional quantum computing, *Front. Phys.* 8 (2020) 479.
- [50] N. Zettili, *Quantum mechanics: concepts and applications*, Wiley Press, 2nd ed., 2010. 623–628, 637–639
- [51] G.R. Malik, R.P. Singh, B.K. Behera, P.K. Panigrahi, First experimental demonstration of multi-particle quantum tunneling in IBM quantum computer, 2019, doi:10.13140/RG.2.2.27260.18569.
- [52] N.M.P. Neumann, Classification using a two-qubit quantum chip, *Quant. Phys.* arXiv:2004.10426 (2020).
- [53] R. Wezeman, N. Neumann, F. Phillipson, Distance-based classifier on QI at, Springer, *Digit. Welt* 4 (2020) 85–91.
- [54] A. Seif, M. Hafezi, C. Jarzynski, Machine learning the thermodynamic arrow of time, *Nat. Phys.* 17 (2021) 105–113.
- [55] H. Blühm, T. Calarco, D. DiVincenzo, *Quantum Technology: Lecture Notes*, in: at 51st IFF Spring School 2020, 2020, p. 20. Chaps. A2, A4–A6, B4
- [56] E.R. Gårding, et al., Bell diagonal: entanglement, non-locality, steering and discord on the IBM quantum computer, *Entropy* 23 (7) (2021) 797.
- [57] G.B. Lesovik, et al., Arrow of time and its reversal on the IBM quantum computer, *Sci. Rep.* 9 (2019) 4396.
- [58] N. Khammassi, I. Ashraf, X. Fu, C. Almudever, K. Bertels, QX: A high-performance quantum computer simulation platform, *IEEE 2017 Design, Automation & Test in Europe Conference & Exhibition* (2017) 464–469.
- [59] P. Zoller, L. Chair, Lecture notes on quantum optics and quantum information, 2005, at: <https://www.lorentz.leidenuniv.nl/lorentzchair/zoller/>, Theor. Phys. Inst., Innsbruck Univ., Austria [Accessed, 2021].
- [60] B.J. Dalton, J. Goold, B.M. Garraway, M.D. Reid, Quantum entanglement for systems of identical bosons, *IOP Phys. Scr.* 92 (2017) 023005.
- [61] Y. Jing, et al., Split spin-squeezed bose-einstein condensates, *N. J. Phys.* 21 (2019) 093038.
- [62] M. Chaudhary, M. Fadel, V. Ivannikov, T. Byrnes, Continuous variable teleportation protocol for split-squeezed bose einstein condensates, *AIP Conf. Proc.* 2241 (2020) 020010.
- [63] T.J.F. Johann, U. Marzolini, Locality and entanglement of indistinguishable particles, *Sci. Rep.* 11 (2021) 15478.
- [64] IBM quantum experience, A quantum computing platform, Qiskit notebooks, and Circuit Composer, 2020, *Quantum phase (shift) gates, QFT and Superdense coding*, a Qiskit notebook [Accessed, 2020].
- [65] QuTech, *Quant. inspire platform*, TU Delft Univ., NE, doc, 2020. *Quant. comp. fact sheet, CR_k, Classification* [Accessed, 2020]
- [66] C. Gidney, Quirk, a quantum circuit simulator, 2020, Examples on quantum teleportation, superdense coding and QFT at: <https://github.com/Strilanc/Quirk> [Accessed, 2020].
- [67] S. Wolfram, Mathematica simulation systems, 2020, at: <https://www.wolframalpha.com> [Accessed, 2015–2020].
- [68] C. Dilmegani, Quantum artificial intelligence, 2021, <https://research.aimultiple.com/quantum-ai> [Accessed, 2021].
- [69] V.N. Pokrovskii, A derivation of the main relations of nonequilibrium thermodynamics, *Hindawi Pub. Corp., UK, ISRN Thermodyn.* 2013 (2013) 906136.
- [70] J.A. Cortese, T.M. Braje, Loading classical data into a quantum computer, *Quant. Phys.* arXiv:1803.01958 and QIP J. (2018).
- [71] S. Deffner, S. Campbell, Quantum thermodynamics, Iop, 2019. Chaps. 1–3. Chap 1.
- [72] J. Diazdelacruz, Quantum relative entropy of tagging and thermodynamics, *Entropy* 22 (2020) 138.
- [73] J. K-Flam, R. Sohal, L. Nie, Information scrambling with conservation laws, *Stat. Mech. arXiv:1805.09607* (2021).
- [74] A. C-Lieta, J.S. Kottmann, A. A-Guzik, Meta-variational quantum eigensolver: learning energy profiles of parameterized hamiltonians for quantum simulation, *Phys. Rev. X Quant.* 2 (2021) 020329.
- [75] S. Lu, M.C. Bañuls, J.I. Cirac, Algorithms for quantum simulation at finite energie, *Phys. Rev. X Quant.* 2 (2021) 020321.
- [76] D. Koch, B. Martin, S. Patel, L. Wessing, P.M. Alsing, Demonstrating NISQ era challenges in algorithm design on IBM's 20-qubit quantum computer, *AIP Adv.* 10 (2020) 095101.
- [77] T.D. Bradley, Ph.D. in Math. and Qaunt. Theo. *What is applied category theory?* A Ph.D. dissertation, Quant. Phys. (2020). 9–11, 22, 43–50, NY Univ., USA (2019); pp. 5–6 of Tensor Product on Qunatum Particles, <https://arxiv.org/abs/2004.05631>.
- [78] Quantiki (Slovak sci. acad.), *Singlet states, Quant. Info.*, 2021, at: <https://www.quantiki.org/wiki/singlet-states> [Accessed, 2021].